Master's thesis

NTNU
Norwegian University of Science and Technology
Faculty of Information Technology and Electrical Engineering
Department of Engineering Cybernetics

Massoud Ibraheem

Model Reduction and Model Predictive Control of Multi-Rotor Wind Turbine

Master's thesis in Industrial Cybernetics

Supervisor: Leif E. Andersson

June 2020

NTNU
Norwegian University of Science and Technology

THE DEPARTMENT OF ENGINEERING
CYBERNETICS (ITK),NTNU

MASTER THESIS

Model Reduction and Model Predictive Control of Multi-Rotor Wind Turbine

Author
MASSOUD IBRAHEEM

Supervisors
LEIF E. ANDERSSON
LARS S. IMSLAND

June 22, 2020

NTNU

Summary

This thesis aims to reduce the order of the models of both the four-rotor turbine and the tower, where the four-rotor turbine was developed by Vestas company. The tower model was reduced from 20 to 17 states using Balanced Truncation and from 20 to 11 states using Matched DC Gain. Then the nonlinear four-rotor turbine model was linearized. The linearized four-rotor model was reduced from 20 to 4 states using the Matched DC Gain method. Two goals should be achieved to reduce the cost of operating the four-rotor turbine in a safe condition. The first goal is to maximize or track the power produced by the turbine. The second goal is to reduce the load on the tower. Thus, there was a need to use modern controllers, such as Model Predictive Control. The Model Predictive Control was developed, and the real-time running were tested. Moreover, the nonlinear Model Predictive Control and linear Model Predictive Control were tested. Different scenarios were used, starting from the full-order nonlinear four-rotor turbine with full-order tower models. Then reduced-order tower used with nonlinear four-rotor turbine, full-order linearized four-rotor turbine and reduced-order turbine. The power tracking, load reduction and real-time optimization were achieved in most scenarios of linear Model Predictive Control. Whereas nonlinear Model Predictive Control could not run in real-time, and the power tracking and load reduction were below requirements.

Keywords: Model reduction, Model Predictive Control, real-time, power tracking, load reduction, Balanced Truncation, Matched DC gain.

Acknowledgments

First of all, I would like to express my sincere thanks and gratitude to my supervisor **Leif Erik Andersson** for his patience, motivation, guidance and immense knowledge. He was ready to guide and help whenever I got stuck. He showed support in everything I do and taught me the right direction for my thesis writing. Leif gave me also the initial code of Model Predictive Control and the polynomial fit. I would like also thank Lars Struen Imsland for his guidance and support.

Besides my supervisors, I would like to thank Jørgen Urdal for giving me a jump start with the multi-rotor. Thanks goes to Felix Rittel for helping in model linearization.

My sincere thanks also go Lionel Sacks for advising about writing the thesis.

My thanks also go to my friends, especially Hilde Grethe Skaret, for supporting and trips in Trondheim in free times during all the works on this thesis.

Last but not least, I would like to thank my family and my fiancee for supporting and encouraging me even they were far away.

Table of Contents

List of Tables

List of Figures

Abbreviations

BT	=	Balanced Truncation
CasADi	=	Computer Algebra Systems Algorithmic Differentiation
DoF	=	Degree of Freedom
FOL	=	Full-Order Linearized
FON	=	Full-Order Nonlinear
FOT	=	Full-Order Tower
Hankel Singular Values	=	HSVs
IEA	=	International Energy Agency
GWEC	=	Global Wind Energy Council
LTI	=	Linear Time-Invariant
LP	=	Linear Programming
MIMO	=	Multi-Input Multi-Output
MDCG	=	Matched DC Gain
MPC	=	Model Predictive Control
NREL	=	National Renewable Energy Laboratory
NMPC	=	Nonlinear Model Predictive Control
NLP	=	NonLineaar Problem
PCA	=	Principal Component Analysis
POD	=	Proper Orthogonal Decomposition
QP	=	Quadratic Programming
RMS	=	Root Mean Square
RMSE	=	Root Mean Square Error
ROL	=	Reduced-Order Linearized
RON	=	Reduced-Order Nonlinear
ROT	=	Reduced-Order Tower
OPC	=	Optimal Control Problem
WECS	=	Wind Energy Converter System
4RT	=	Four-Rotor Turbine

Chapter 1

Introduction

1.1 Motivation and importance of wind energy

Energy plays a vital role in the development of human society. From coal, gas to oil, and renewable energy, man has made transitions according to technical development. The energy demand has been rising in the last few years. This increasing demand calls for a sustainable and clean energy resources that would reduce the load on non-renewable resources according to the international energy agency (IEA) [11]. Wind energy is one of the most popular renewable energy sources, where the popularity of using the energy in the wind has always fluctuated with the price of fossil fuels. Fig.1.1 shows how the global wind power production increased over the years. Wind power offers many advantages, which explains why it is the fastest-growing energy source in the world. These advantages offer a clean fuel source, relying on the renewable power of the wind, the lowest-priced renewable energy technology available today. Another advantage is the fact that wind turbines can be built on farms or ranches, thus benefiting the economy in rural areas. To get a better use of turbine capacity as well as the alleviation of aerodynamic and mechanical loads, new control technologies play a significant role in modern wind turbines. Real-time control is an essential issue for controllers. Therefore, there is a requirement for a model reduction to achieve real-time control.

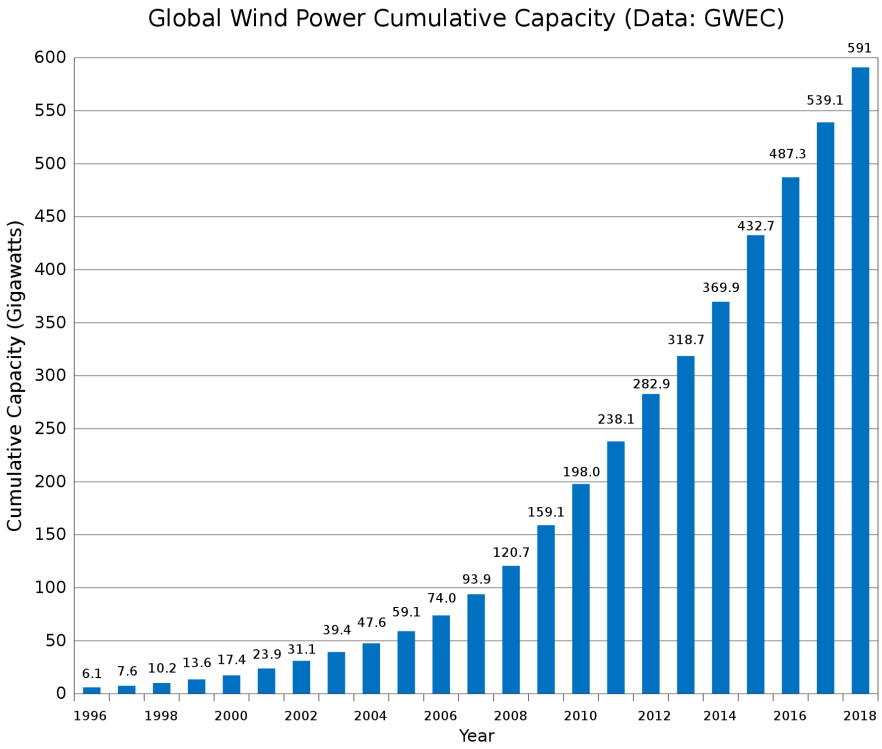

Figure 1.1: Global wind power cumulative capacity [25].

1.2 Problem definition

The main objectives of this work are the model reduction of the four-rotor turbine model and the tower model. A nonlinear MPC (NMPC) and a linear MPC will be developed, where the nonlinear MPC and linear MPC should run in real-time optimization. Finally, the power tracking and load reduction on the tower will be achieved.

1.3 Contributions

The contributions are as follows:

- The interpolation and polynomial method of power coefficient and thrust coefficient were created and tested.
- The wind profile with mean wind speed (14 $m.s^{-1}$) was created.

- The nonlinear MPC (NMPC) was developed and tested for both constant and turbulent wind speeds. The power tracking, load reduction on the tower, and real-time optimization were tested.
- The four-rotor turbine (4RT) was linearized and reduced from 20 states to 4 states with Matched DC Gain (MDCG) method. Additionally, the tower model was reduced from 20 states to 17 states using the Balanced Truncation (BT) method. Then the tower model was reduced from 20 states to 11 states with Matched DC Gain (MDCG). The simulation was done for both full-order and reduced-order for both 4RT and tower models.
- Linear MPC with constant wind speed was developed and tested. Different scenarios were implemented. The power tracking, load reduction on the tower, and real-time optimization were tested.

Chapter 2

Background

This chapter includes the theory part of this thesis, which provides the explaining, deriving, and figures of the necessary concepts and equations.

2.1 Wind energy

A wind turbine is a revolving machine that captures part of the kinetic energy from the wind, converting it into mechanical energy. This mechanical energy is then converted into electricity sent to a power grid. The turbine components responsible for these energy conversions are the rotor and the generator. That is why the wind turbine is named a Wind Energy Converter System (WECS) [3]. The aerodynamic power captured by the rotor is given by the following equation as:

$$P_r = \frac{1}{2}\rho\pi R^2 V_{rot}^3 C_p(\lambda, \beta), \tag{2.1}$$

where P_r denotes rotor power, R is the rotor radius, ρ is the air density, V_{rot} is the wind speed over rotor, C_P the aerodynamic power coefficient, β is pitch angle, Ω rotor speed and λ is tip-speed-ratio, where $\lambda = \frac{\Omega R}{V}$. Different control methods are used to either optimize or limit power output by minimizing the cost of supplied energy. This can be done by controlling the blade angle adjustment, which will lead to adjust the rotor speed and the generator speed. However, there are limitations on power and speed below some values to prevent the turbine from unsafe operations under high wind conditions [3].

2.2 Power coefficient C_P and thrust coefficient C_T

The power coefficient is of special interest for control purposes and the relation between C_P and torque coefficient C_Q is:

$$C_P = C_Q/\lambda \tag{2.2}$$

The two coefficients(C_p and C_T) are written in terms of the pitch angle β and the so-called tip-speed-ratio λ defined as:

$$\lambda = \frac{\Omega R}{V_{rot}} \tag{2.3}$$

The tip-speed ratio is the ratio of the linear speed of the blade tip to the wind speed over rotor V_{rot}, where R is fixed for a given turbine, λ is time-varying for a variable-speed turbine.

For modern wind turbines, the relationship between the power coefficient C_P and the tip-speed ratio λ is a nonlinear function. C_P also depends on the blade pitch angle β in a nonlinear fashion. Similarly, the relationship between the thrust coefficient C_t and both the tip-speed ratio λ and the blade pitch angle β is nonlinear.

In the case of fixed-pitch wind turbines, C_P varies only with λ, since β = 0. On the other hand, the maximum conversion efficiency is obtained at an optimum tip-speed ratio λ_o. In the case of fixed-speed wind turbines, the turbines will operate with maximum efficiency just for a single wind speed, whereas variable-speed turbines can work with maximum efficiency over a wide wind speed range up to rated power. To realize the benefits of variable-speed operation, the rotational speed must be adjusted to the wind speed to maintain an optimum tip-speed-ratio [3].

In the case of variable-pitch wind turbines, the maximum power coefficient can be achieved by tuning λ and β where the pitch angle β is adjusted by a pitch angle actuator. In this thesis, the dynamics of the pitch angle β is taken to be:

$$\dot{\beta} = \frac{1}{\tau_b}(\beta_{ref} - \beta), \tag{2.4}$$

where τ is time constant pitch actuator and β_{ref} is desired pitch angle, which is one of the MPC's inputs for each individual turbine. The pitch angle is subject to constraints:

$$\beta_{min} < \beta < \beta_{max}. \tag{2.5}$$

In this thesis:

$$0^\circ < \beta < 20^\circ$$

The data table of wind turbine 5 MW is obtained from National Renewable Energy Laboratory(NREL), where the individual wind turbine must be rated at 5 MW. However, there

are two methods of how the C_P and C_T lookup table is handled. The interpolation and the nonlinear polynomial methods are derived based on numerical tables of NREL wind turbine. In this thesis, for the interpolation and the polynomial methods, the pitch angle is restricted to the interval $0° \leq \beta \leq 20°$ and the tip-speed ratio is restricted to the interval $4.5 \leq \lambda \leq 17.5$. Fig. 2.1 shows the curve of the power coefficient and thrust coefficient for interpolation method of a 5 MW wind turbine where the maximum value of power coefficient is $C_{P_{max}} = 0.48$ at pitch angle $\beta = 0$ and $\lambda = 7.6$ and the maximum value of thrust coefficient is $C_{T_{max}} = 1.19$ at pitch angle $\beta = 0$ and $\lambda = 17.5$. Note that the negative values of C_p and C_T are removed in fig. 2.1.

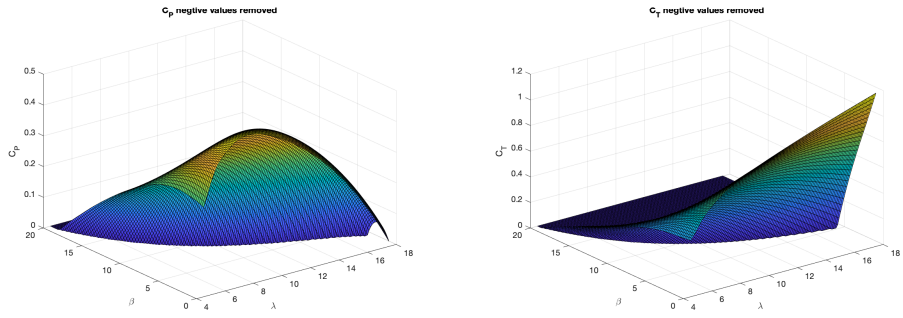

(a) Power coefficient for interpolation method

(b) Thrust coefficient for interpolation method

Figure 2.1: Power and thrust coefficient for interpolation method

The nonlinear polynomial for power coefficient creates a surface fit to the data in vectors of pitch β, tip-speed ratio λ, and power coefficient C_P by using nonlinear polynomial surface (poly54). Poly54 is chosen because it gave an acceptable error between fitted data and interpolated data.
The estimated nonlinear polynomial is formulated as follows:

$$\begin{aligned} C_P(\beta,\lambda) =& pp_{00} + pp_{10}\beta + pp_{01}\lambda + pp_{20}\beta^2 + pp_{11}\beta\lambda + pp_{02}\lambda^2 + pp_{30}\beta^3 + pp_{21}\beta^2\lambda \\ &+ pp_{12}\beta\lambda^2 + pp_{03}\lambda^3 + pp_{40}\beta^4 + pp_{01}\lambda + pp_{31}\beta^3\lambda + pp_{22}\beta^2\lambda^2 + pp_{02}\lambda^2 \\ &+ pp_{13}\beta\lambda^3 + pp_{04}\lambda^4 + pp_{50}\beta^5 + pp_{41}\beta^4\lambda + pp_{32}\beta^3\lambda^2 + pp_{23}\beta^2\lambda^3 \\ &+ pp_{14}\beta\lambda^4, \end{aligned} \tag{2.6}$$

where $pp_{00}, pp_{01}, \ldots, pp_{14}$ are coefficients of the C_P polynomial.

The nonlinear polynomial for the thrust coefficient is formulated as:

$$\begin{aligned} C_T(\beta,\lambda) =& pt_{00} + pt_{10}\beta + pt_{01}\lambda + pt_{20}\beta^2 + pt_{11}\beta\lambda + pt_{02}\lambda^2 + pt_{30}\beta^3 + pt_{21}\beta^2\lambda \\ &+ pt_{12}\beta\lambda^2 + pt_{03}\lambda^3 + pt_{40}\beta^4 + pt_{01}\lambda + pt_{31}\beta^3\lambda + pt_{22}\beta^2\lambda^2 + pt_{02}\lambda^2 \\ &+ pt_{13}\beta\lambda^3 + pt_{04}\lambda^4 + pt_{50}\beta^5 + pt_{41}\beta^4\lambda + pt_{32}\beta^3\lambda^2 + pt_{23}\beta^2\lambda^3 \\ &+ pt_{14}\beta\lambda^4, \end{aligned} \tag{2.7}$$

where $pt_{00}, pt_{01}, \ldots, pt_{14}$ are coefficients of the C_T polynomial.
The graph of C_P and C_T function is shown in fig. 2.2 where the maximum power coefficient for the fitted data is $C_{P_{maxfit}} = 0.48$ at pitch angle $\beta = 0.2$ and $\lambda = 7.7$ and the maximum thrust coefficient for the fitted data is $C_{T_{maxfit}} = 1.17$ at pitch angle $\beta = 0$ and $\lambda = 17.5$. Note that the negative values of C_p and C_T are removed in fig. Fig. 2.2.

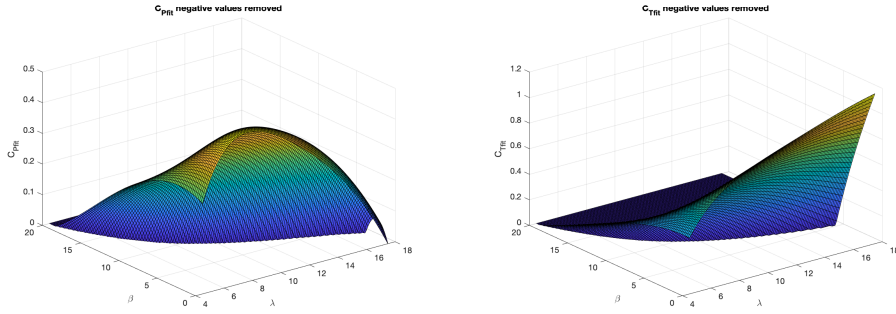

(a) Power coefficient for polynomial method **(b)** Thrust coefficient for polynomial method

Figure 2.2: Power and thrust coefficient for polynomial method

The absolute error in fit for C_P and C_T shows in fig.2.3

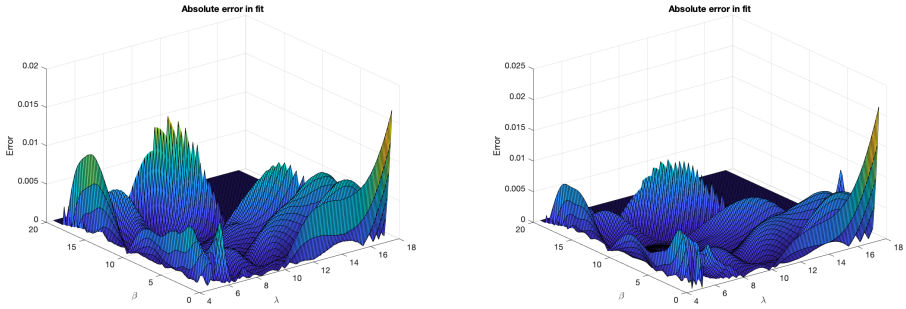

(a) Absolute error in fit of the power coefficient

(b) Absolute error in fit of the thrust coefficient

Figure 2.3: The absolute error in fit of power and thrust coefficient

Since the Casadi package for optimization is used in this thesis, and numerical experiments showed that the polynomial method is faster in the optimization than the interpolation method.

2.3 Control objectives

Minimizing the cost of the energy that is captured from the wind requires achieving three goals.

- The first goal is the maximization of energy capture or tracking the power reference, taking into consideration both physical and economic constraints, such as cut-in wind speed, cut-out wind speed, rated power and rated wind speed. Fig. 2.4 shows the ideal power curve with three operation regions, where the plot was obtained by running $openFAST$ simulator and the idea was inspired from [16]. At the region before region I, the wind speed is lower than the cut-in wind speed V_{cut-in}. Thus, the power available in the wind is low compared to losses in the turbine system, so the turbines dot not operate and are stopped from rotating by a mechanical brake. Whereas the wind speed at the region I is not strong enough to produce rated power,i.e., lower than rated wind speed V_{rated} , and the available power is lower than rated power [3]. Maximizing the captured power, in the operational region I, requires maximizing the following equation:

$$P_r = \frac{1}{2}\rho\pi R^2 V_{rot}^3 C_P(\lambda, \beta) \tag{2.8}$$

The power maximizing can also done in the following equation:

$$P_r = \omega M_{gen}, \tag{2.9}$$

where R is the rotor radius, ρ is the air density, V_{rot} is the wind speed over the rotor, the aerodynamic power coefficient C_P determines how much of the total amount of available power in the rotor disc is transferred from the wind to the rotor, which represents the percentage of power, ω is the generator speed, and M_{gen} is the generator torque. Maximum power can be captured by operating the turbines with a maximum power coefficient C_{Pmax}. This can be achieved by holding the pitch angle at the optimal position and controlling the generator torque to keep the turbine speed closest to the one that will assure optimal tip speed ratio.
While Region II, is a transition region between the optimum power curve (region I) and the constant power line (region III). The objective in this region is to reach the rated power when approaching the rated wind speed. Finally, in region III, where the wind speed is higher than V_{rated}, the goal is to limit the generated power equal to or below its rated value, so that safe electrical and mechanical loads are not exceeded. Therefore the turbine must be operated at a power coefficient lower than maximum power coefficient $C_{P_{max}}$[26]. That can be achieved by pitching the blades or by yawing the turbine out of the wind. The aerodynamic power P_r is related to rotor speed Ω and aerodynamic torque T_r by

$$P_r = T_r \Omega \tag{2.10}$$

If the power and rotor speed is held constant, the aerodynamic torque must also be constant even as wind speed varies [19].

- The second goal is to protect the turbine from mechanical loads. The dynamic loads that include changes in the aerodynamic torque that affect the drive-train and changes in the aerodynamic loads that affect the mechanical structure. Moreover, there are other kinds of dynamic loads, such as the load induced by turbulence, so-called transient load, and those that induce high-frequency cyclic loads [3]. The controllers must provide damping at the vibration modes in order to alleviate high-frequency loads and reduce the risk of fatigue breakdown.

- The third and final goal is power quality, which includes conditioning the generated power to comply with interconnection standards [3]. Nevertheless, the power quality

will not be taken into consideration in this thesis.

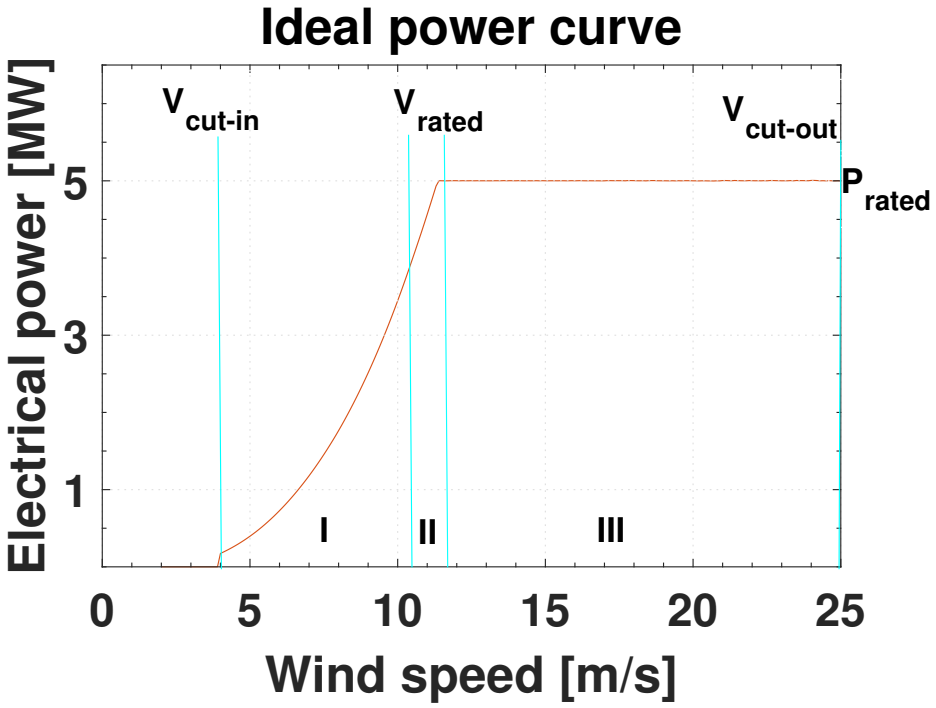

Figure 2.4: Ideal power curve.

2.4 Multi-rotor wind turbine model

The need for more energy caused an increase in the size of wind turbines over the last years. That is why the radius and cost of these large turbines are increased. However, the weight increases by the cube of the rotor radius R while the power increases by the square of the rotor radius R. Thus, the cost increases faster than the power gained. To remedy these challenges, a multi-rotor wind turbine could be considered, which consists of numbers of small rotors to produce the same amount of power [14, 24]. The concept of a multi-rotor wind turbine that used in Vestas Wind Systems is to mount four rotors and generators to the same structure that consists of a tower with arms, as shown in fig. 2.5, where each turbine is 5 MW NREL as in [13] . There are many benefits of multi-rotor turbines. Firstly, reducing the weight of components compared to conventional turbines. Secondly, more power and aerodynamic efficiency due to smaller components, which improves the power curve up to rated power. Finally, reducing transportation challenges and costs due to smaller size and less weight [12, 24].

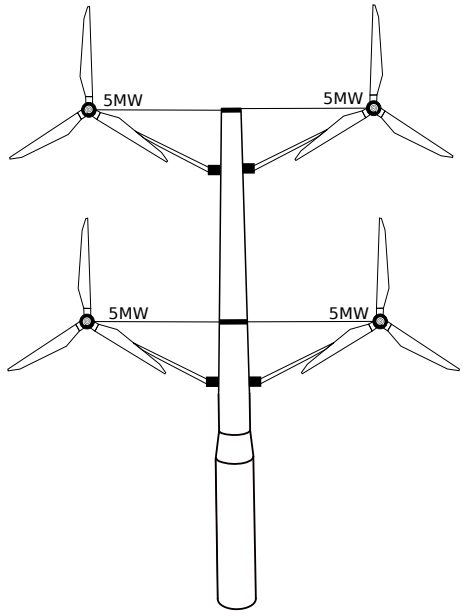

Figure 2.5: Four-rotor turbine (4RT).

Wind turbines are complex mechanical systems where the aerodynamic forces induced by the wind passing through the rotors are highly nonlinear. These nonlinearities lead to significant variations in the dynamic behavior of the systems. Therefore, their modeling is complex.

2.4.1 Nonlinear model of the four-rotor turbine

Four-Rotor Turbine (4RT) consists of four simple turbines which is modeled as in [9]. The number of total states for the whole model included the tower model are 40. The states are divided to 20 states describing 4RT model and 20 states describe structural model. The states for each one rotor turbine are rotor speed Ω_i, generator speed ω_i, shaft torsion angle ϕ_i, generator torque M_{gen_i}, pitch angle β_i, where $i = 1 \dots 4$. The inputs for each rotor turbine are power reference P_{ref_i} and pitch reference β_{ref_i}, and the output is tower thrust F_{tow_i} for each rotor turbine. Parameters that used are air density ρ, rotor radius R, gear ratio N, torsion spring constant K_{shaft}, viscous friction B_{shaft}, rotor inertia I_{rot}, generator inertia I_{gen}, time constant generator τ_g and time constant pitch actuator τ_b.
The aerodynamics of the 4RT are described as follows

$$M_{shaft_i} = \frac{1}{2}\rho\pi R^2 V_{rot}^3 C_P(\lambda_i, \beta_i)\Omega_i^{-1}, \tag{2.11a}$$

$$F_{tow_i} = \frac{1}{2}\rho\pi R^2 V_{rot}^2 C_T(\lambda_i, \beta_i)\Omega_i^{-1}, \tag{2.11b}$$

where M_{shaft_i} are main shaft torque for each individual single rotor turbine, F_{tow_i} are thrust force for each individual single rotor turbine, C_P and C_T are two look-up tables with inputs tip speed ratio ($\lambda_i = R\Omega_i/V_{rot}$) and pitch angle.

The drive train model for each rotor turbine is given by:

$$\dot{\Omega}_i = \frac{1}{I_{rot}}(M_{shaft_i} - \phi_i K_{shaft} - \dot{\phi}_i B_{shaft}), \tag{2.12}$$

$$\dot{\omega}_i = \frac{1}{I_{gen}}(-M_{gen_i} + \frac{1}{N}(\phi_i K_{shaft} + \dot{\phi}_i B_{shaft})) \tag{2.13}$$

$$\dot{\phi}_i = \Omega_i - \frac{1}{N}\omega_i, \tag{2.14}$$

The generator torque is described as:

$$\dot{M}_{gen_i} = \frac{1}{\tau_{gen}}(\frac{P_{ref_i}}{\omega_i} - M_{gen_i}), \tag{2.15}$$

The pitch angle dynamics is:

$$\dot{\beta}_i = \frac{1}{\tau_b}(\beta_{ref_i} - \beta_i). \tag{2.16}$$

2.4.2 Linear model of the Four-Rotor Turbine (4RT)

To find linearized models of the nonlinear system around operating points, Taylor series expansion is used. Consider the nonlinear differential equation [22]:

$$\dot{\boldsymbol{x}}(t) = f(\boldsymbol{x}(t), \boldsymbol{u}(t)), \tag{2.17}$$

where f is a function, $\boldsymbol{x}(t)$ is the state vector, and $\boldsymbol{u}(t)$ is the input vector. Let ($\bar{\boldsymbol{x}}$,$\bar{\boldsymbol{u}}$) be the operating points, which is not necessary to be the equilibrium point of the system. Starting from the idea that the linearized model is working well around the operating points, the

difference between $\boldsymbol{x}$ and $\bar{\boldsymbol{x}}$, and $\boldsymbol{u}$ and $\bar{\boldsymbol{u}}$ are defined as follows:

$$\begin{aligned} \boldsymbol{\Delta x}(t) &= \boldsymbol{x}(t) - \bar{\boldsymbol{x}} \\ \boldsymbol{\Delta u}(t) &= \boldsymbol{u}(t) - \bar{\boldsymbol{u}} \end{aligned} \tag{2.18}$$

By inserting the equations 2.18 in equation 2.17:

$$\dot{\boldsymbol{\Delta}}\boldsymbol{x}(t) = f\left(\bar{\boldsymbol{x}} + \boldsymbol{\Delta x}(t), \bar{\boldsymbol{u}} + \boldsymbol{\Delta u}(t)\right) \tag{2.19}$$

Using Taylor series expansion and neglect higher order than the first-order gives:

$$\dot{\boldsymbol{x}}(t) \approx f(\bar{\boldsymbol{x}}, \bar{\boldsymbol{u}}) + \left.\frac{\partial f}{\partial x}\right|_{\substack{x=\bar{x} \\ u=\bar{u}}} \boldsymbol{\Delta x}(t) + \left.\frac{\partial f}{\partial u}\right|_{\substack{x=\bar{x} \\ u=\bar{u}}} \boldsymbol{\Delta u}(t), \tag{2.20}$$

where $\dot{\boldsymbol{\Delta}}\boldsymbol{x}(t) = \dot{\boldsymbol{x}}(t)$. The Jacobian matrices can be defined as:

$$\boldsymbol{A} = \left.\frac{\partial f}{\partial x}\right|_{\substack{x=\bar{x} \\ u=\bar{u}}} \quad , \quad \boldsymbol{B} = \left.\frac{\partial f}{\partial u}\right|_{\substack{x=\bar{x} \\ u=\bar{u}}} \tag{2.21}$$

The Jacobian linearization is obtained:

$$\dot{\boldsymbol{x}}(t) = f(\bar{\boldsymbol{x}}, \bar{\boldsymbol{u}}) + \boldsymbol{A\Delta x}(t) + \boldsymbol{B\Delta u}(t) \tag{2.22}$$

The system is linearized at different parameter values p, where the parameter is the mean wind speed. Several coherent Linear Time-Invariant (LTI) systems are found for different mean wind speed as follows:

$$\dot{\boldsymbol{x}}(t) = f(\bar{\boldsymbol{x}}, \bar{\boldsymbol{u}}) + \boldsymbol{A}_p\boldsymbol{\Delta x}(t) + \boldsymbol{B}_p\boldsymbol{\Delta u}(t) \tag{2.23a}$$

$$\boldsymbol{y}(t) = \boldsymbol{C}_p\boldsymbol{\Delta x}(t) + \boldsymbol{D\Delta u}(t), \tag{2.23b}$$

where:

$\boldsymbol{x}$ -the state vector;
$\boldsymbol{A}_p$-the system matrix corresponding to mean wind speed p;
$\boldsymbol{B}_p$-the control matrix corresponding to mean wind speed p;
$\boldsymbol{u}$ -the input control;
$\boldsymbol{y}$ -the output of the system;
$\boldsymbol{C}_p$-the output matrix corresponding to mean wind speed p;

2.4.3 Structural model

A challenge in using a multi-rotor wind turbine is the structural complexity. Increasing of structural complexity can cause increases in fatigue loads [15, 12]. However, the equations of motion derivation of the structural model is explained in detail in [15]. Here follows a short summary of the way of deviation. To derive the equation of motion, Lagrange equations with 10 Degrees of Freedom (DoFs) are used with some assumptions. The following assumptions are considered

- No gravitational loads
- No aerodynamic stiffening and damping from rotors
- The only generalized force is thrust force
- Very stiff arms
- Blades are not in the model
- Ten generalized coordinates

The DoFs include two rotational components, lower section rotation $\theta_{xP0}(t)$ and upper section rotation $\theta_{xP1}(t)$ and two translation components, $u_{yP0}(t)$ and $u_{yP1}(t)$. where $P0$ and $P1$ refers to the lower platform and the upper platform, respectively. Each two rotor mounts on one platform. $\theta_{zP0}(t)$ and $\theta_{zP1}(t)$ are two DoFs represent tower torsion of each platform. Furthermore, four DoFs represent arm torsion $\theta_{xR1}(t), \theta_{xR2}(t), \theta_{xR3}(t)$ and $\theta_{xR4}(t)$. Where $R1, R2, R3$ and $R4$ refer to each nacelle.
The Lagrangian equation of motion L is formulated as:

$$L(\boldsymbol{q}, \dot{\boldsymbol{q}}, t) = T(\boldsymbol{q}, \dot{\boldsymbol{q}}, t) - U(\boldsymbol{q}), \tag{2.24}$$

where T is kinetic energy, U is potential energy and $\boldsymbol{q}$ is generalized coordinates where $\boldsymbol{q} = [\theta_{zP0}, \theta_{zP1}, u_{yP0}, u_{yP1}, \theta_{xP0}, \theta_{xP1}, \theta_{xR1}, \theta_{xR2}, \theta_{xR3}, \theta_{xR4}]^T$.
The equation of motion is:

$$\frac{d}{dt}\left(\frac{\partial L}{\partial \dot{q}_i}\right) - \frac{\partial L}{\partial q_i} = \tau_i^{(n)}, \quad i = 1, 2, \ldots, n \tag{2.25}$$

where $\tau_i^{(n)}$ is generalized forces and n is the number of generalized coordinates which is ten in our case. The generalized force can be formulated as:

$$\tau_i^{(n)} = \sum_k \left(F_{xk}\frac{\partial x_k}{\partial q_i} + F_{yk}\frac{\partial y_k}{\partial q_i} + F_{zk}\frac{\partial z_k}{\partial q_i} \right), \tag{2.26}$$

where F_{xk}, F_{yk} and F_{zk} are the external thrust forces come from the rotors which acting on the tower, k is number of the forces that affecting on the tower.
By inserting values of T, U and $\tau_i^{(n)}$ in 2.25 and linearizing around zero, the linear model is obtained:

$$\mathbf{M_s}\ddot{\mathbf{q}} + \mathbf{C}\dot{\mathbf{q}} + \mathbf{K_s}\mathbf{q} = \mathbf{F}, \tag{2.27}$$

where $\boldsymbol{M_s}$ is the mass matrix, $\boldsymbol{C}$ is the damping matrix, $\boldsymbol{K_s}$ is the stiffness matrix, $\boldsymbol{F}$ the force vector.
From equation 2.26, the state space can be obtained:

$$\dot{\boldsymbol{x}} = \mathbf{A}\mathbf{x} + \mathbf{B}\mathbf{u}, \tag{2.28}$$

where $\boldsymbol{x} = [\boldsymbol{q}, \dot{\boldsymbol{q}}]^T$ is the state vector, $\boldsymbol{u} = [F_{tow_1}, F_{tow_2}, F_{tow_3}, F_{tow_4}]^T$ is the input vector which includes the rotor thrust forces, $\boldsymbol{B}$ is the input matrix and

$$\mathbf{A} = \begin{bmatrix} \mathbf{0} & \mathbf{I} \\ -\mathbf{M_s}^{-1}\mathbf{K_s} & -\mathbf{M_s}^{-1}\mathbf{C} \end{bmatrix} \tag{2.29}$$

is the system matrix.

2.4.4 Load calculation

The objective function for optimization problem consists of two terms. The first term is the power which is maximized or tracked the power reference and the second term is the loads on tower structure which is minimized. However, the load is calculated as follows:

$$\boldsymbol{L}_{tow} = \boldsymbol{M}_s\ddot{\boldsymbol{q}} + \boldsymbol{K}_s\boldsymbol{q}, \tag{2.30}$$

where $\boldsymbol{L}_{tow} \in \mathbb{R}^{10\times 1}$ is the loads on the tower structure and $\boldsymbol{q} \in \mathbb{R}^{10\times 1}$ is the state vector.

2.4.5 Objective function

The control objective for the multi-rotor is to minimize the fatigue in the structure supporting the nacelles while maximizing generated power. Thus, the nonlinear objective function is written as follows:

$$-\frac{1}{2}P'_{tot}Q_pP_{tot} + \frac{1}{2}\boldsymbol{L}'_{tow}\boldsymbol{Q}_l\boldsymbol{L}_{tow}, \tag{2.31}$$

where $\boldsymbol{P}_{tot} = \omega_1 M_{gen1} + \omega_2 M_{gen2} + \omega_3 M_{gen3} + \omega_4 M_{gen4}$ is the sum of the powers generated from the four turbines, $Q_p > 0$ is the power's weight and $\boldsymbol{Q}_l$ is the diagonal

matrix of the load's weight, where all diagonal elements are positive.
The convexity of the optimization problem is important for real-time optimization. The problem called to be convex if the objective function and the constraints are convex. The objective function is convex for the Quadratic Programming (QP) if the weight matrices are positive definite, where the Linear Programming (LP) problem is convex. If the constraints are linear, i.e., the linear model is used and assuming other constraints are linear, that gives the convex optimization problem. In the contract, if the constraints are nonlinear (nonlinear model is used), the optimization problem is non-convex. The basic difference between the convexity and non-convexity optimization is that in convex optimization, the local optimal is the global optimal solution. Whereas, the non-convex optimization may have multiple locally optimal points, and it can take much time to identify whether the problem has no solution or if the solution is global. Thus, the convexity is important to optimization problem because it speeds up the optimization problem. Thus, it makes the optimization runs in real-time. However, in this thesis, the objective function in 2.31 is non-convex; this leads to the non-convex optimization problem. Nevertheless, the linear model (the constraint for optimization problem) speeds up the computational time.

2.4.6 Ambient wind field

The wind input can vary substantially in space. The deviations of the wind speed from the expected nominal wind speed across the rotor plane are considered disturbances for control design. It is difficult to obtain a good measurement of the wind speed because of the spatial and temporal variability, the rotor's interactions, and changes in the wind input. Not only does turbulent wind causes the wind to be different for the various blades, but the wind speed input is different at different positions along each blade. In this thesis, Wind field is created using $gen\_windfield.m$ in [1] where this method needs some data listed below:

- Mean wind speed (U_0)
- Turbulence intensity (T_i)
- Grid resolution (d)
- The length of the wind field (L_x)
- The width of the wind field (L_y)
- The maximum simulation time (T_s)

The four single rotor turbines are spaced equally with 10% of the rotor diameter. The wind speed changes with altitude where wind speed increases with increasing altitude and wind

speed decrease close the Earth's surface, which it calls wind shear.
Wind shear can be written as

$$u/u_0 = (h/h_0)^{\alpha}\,, \tag{2.32}$$

where:
u-the wind speed at height h;
u_0-the wind speed at height h_0;
α-the wind shear exponent
The wind shear contribution is added to wind profile for top rotors for this purpose.

2.5 Model reduction

In many engineering situations, the dynamic models are of high mathematic order, which introduces complexity for computation and storage. This makes those models not suitable for an application like optimization and control design purposes. To avoid these challenges, model reduction is used. The model reduction produces a reduced-order model from the full order model that arises from physics-based modeling by keeping the states that capture most of the input to the output dynamics of the full dynamic systems. Hence reduced-order model can be used in the design of the control systems, optimization, and analysis. The reduction model gives faster predictions, which gives faster control [23].

2.5.1 Reduced-order model criteria

There are many methods used for model reduction, and several criteria should be considered to choose the appropriate method. The main criteria that are considered are [6]:

- **Minimal computational cost:** The computational cost must be low enough to provide the real-time signals in an operational context.
- **Physical meaning:** Many algorithms focus on the relation between inputs and outputs without preserving the physical meaning of the reduced-order states. However, the physical meaning helps to understand the change in the states.
- **Input and output relations:** Some methods do not consider the input and output relationships such as Principal Component Analysis (PCA) and Proper Orthogonal Decomposition (POD). On the other side, some of them are designed to create input and output relationships such as Balanced Truncation (BT) and Matched DC Gain

(MDCG). More accuracy of reduced-order model can be obtained, if the relationships between input and output takes into consideration.

There are many reduction methods, some of them used to reduce the nonlinear models, and some used to reduce the linear models.
Given a nonlinear full order model for a multiple-input multiple-output (MIMO) system

$$\dot{\boldsymbol{x}}(t) = f(\boldsymbol{x}(t), \boldsymbol{u}(t), t) \tag{2.33a}$$

$$\boldsymbol{y}(t) = h(\boldsymbol{x}(t), \boldsymbol{u}(t), t), \tag{2.33b}$$

where:

$\boldsymbol{x}$-the state vector;

$\boldsymbol{u}$-the input control;

$\boldsymbol{y}$-the output of the system;

$\boldsymbol{x} \in \mathbb{R}^{\boldsymbol{n_x}}, \boldsymbol{u} \in \mathbb{R}^{\boldsymbol{n_u}}, \boldsymbol{y} \in \mathbb{R}^{\boldsymbol{n_y}}$.

n_x, n_u, n_y-the numbers of states, inputs and outputs, respectively;

The nonlinear reduced-order model can be described as following:

$$\dot{\boldsymbol{x}}_r(t) = f_r(\boldsymbol{x}_r(t), \boldsymbol{u}(t), t) \tag{2.34a}$$

$$\boldsymbol{y}_r(t) = h_r(\boldsymbol{x}_r(t), \boldsymbol{u}(t), t), \tag{2.34b}$$

where:

$\boldsymbol{x}_r$-reduced state;

$\boldsymbol{u}$-input;

$\boldsymbol{y}_r$-output corresponding to reduced state;

$\boldsymbol{x}_r \in \mathbb{R}^{n_r}$, $\boldsymbol{u} \in \mathbb{R}^{n_u}$,$\boldsymbol{y} \in \mathbb{R}^{n_y}$, $n_r \ll n_x$.

n_r, n_u, n_y-the numbers reduced states, inputs and outputs, respectively;

By linearizing the nonlinear model in 2.33 around equilibrium points or operating points, the state-space model (linearized model) is acquired. The equations in 2.35 and 2.36 describe the full order model and reduced order model for a multiple-input multiple-output (MIMO) system, respectively.

$$\dot{\boldsymbol{x}}(t) = \boldsymbol{A}\boldsymbol{x}(t) + \boldsymbol{B}\boldsymbol{u}(t) \tag{2.35a}$$

$$\boldsymbol{y}(t) = \boldsymbol{C}\boldsymbol{x}(t) + \boldsymbol{D}\boldsymbol{u}(t), \tag{2.35b}$$

where $\boldsymbol{A} \in \mathbb{R}^{\boldsymbol{n_x} \times \boldsymbol{n_x}}, \boldsymbol{B} \in \mathbb{R}^{\boldsymbol{n_x} \times \boldsymbol{n_u}}, \boldsymbol{C} \in \mathbb{R}^{\boldsymbol{n_y} \times \boldsymbol{n_x}}, \boldsymbol{D} \in \mathbb{R}^{\boldsymbol{n_y} \times \boldsymbol{n_u}}$.

$$\dot{\boldsymbol{x}}_r(t) = \boldsymbol{A}_r\boldsymbol{x}_r(t) + \boldsymbol{B}_r\boldsymbol{u}(t) \tag{2.36a}$$

$$\boldsymbol{y}_r(t) = \boldsymbol{C}_r\boldsymbol{x}_r(t) + \boldsymbol{D}_r\boldsymbol{u}(t), \tag{2.36b}$$

where $\boldsymbol{A}_r \in \mathbb{R}^{n_r \times n_r}, \boldsymbol{B}_r \in \mathbb{R}^{n_r \times n_u}, \boldsymbol{C}_r \in \mathbb{R}^{n_y \times n_r}, \boldsymbol{D}_r \in \mathbb{R}^{n_y \times n_u}, n_r \ll n_x$.

2.5.2 Reduction methods

Two methods are used to reduce the order of the linear model. Balanced Truncation (BT) and Matched DC Gain (MDCG) methods are selected to reduce the order of model due to the advantages of these two methods, such as using linear models and the relation between input and output.

2.5.2.1 Balanced Truncation method

Balanced Truncation (BT) can be used to reduce the order of the full-order linear models as in 2.35 to get the reduced-order model in 2.36 such that the reduced-order model is close, in some sense as in section 2.5.3, to the full-order model. In general, the BT can give more accuracy in fast transients than low-frequency dynamics. Moreover, BT is connected to the controllability and observability. A system is called controllable if there exists an input $u(t), t_0 \leq t \leq t_1$, that transfers the state of the system from the initial states $x\left(t_0\right) = x_0$ to the other state $x\left(t_1\right) = x_1$ in a finite time interval. Also, a system is called observable if the value of the initial state can be determined from the system output $y(t)$ that has been observed through the time interval $t_0 \leq t \leq t_1$, for a finite time interval.
The balanced truncation (BT) [4, 21, 18] finds the states that balance the controllability and observability of those states. Thus, keeping the states which will be easy to control and observe and truncating those states that are uncontrollable and unobservable. The principle is to get balance realization or internally balanced realization by doing coordinate transformations from original coordinate $\boldsymbol{x}$ to new coordinate $\tilde{\boldsymbol{x}}$

$$\tilde{\boldsymbol{x}}(t) = \boldsymbol{T}\boldsymbol{x}(t), \tag{2.37}$$

where T is an invertable matrix.
The transformation ensures that the controllability and observability Gramians of the transformed system are the same and equal to diagonal matrix $\boldsymbol{\Sigma}$ as we will see later. Where the diagonal elements are the Hankel Singular Values (HSVs) of the system

$$\sigma_1 \geq \sigma_2 \geq \cdots \geq \sigma_{n_x} \geq 0$$

The Hankel Singular Values (HSVs) are arranged in decreasing order and provide a measure of energy for every state in a system and they are the square root of the eigenvalues of the product of controllability and observability Gramians $\boldsymbol{W_c}$ and $\boldsymbol{W_o}$ of the original system and given by

$$\sigma_i = \sqrt{\lambda_i \left(\boldsymbol{W_c W_o}\right)}, \tag{2.38}$$

where $i = 1, 2, ..., n_x$
The controllability $\boldsymbol{W_c}$ and observability $\boldsymbol{W_o}$ gramians matrices for the original linear system in equations 2.35 defines as follows

$$\boldsymbol{W_c} = \int_0^\infty \boldsymbol{e^{At} B B^T e^{A^T t} dt} \tag{2.39}$$

is called controllability gramians

$$\boldsymbol{W_o} = \int_0^\infty \boldsymbol{e^{A^T t} C^T C e^{At} dt} \tag{2.40}$$

is called obsorvabelly gramians
The matices $\boldsymbol{W_c}$ and $\boldsymbol{W_o}$ can be also calculated form the Lyapunov equation as follows

$$\boldsymbol{A W_c + W_c A^T + B B^T = 0} \tag{2.41}$$

$$\boldsymbol{W_o A + A^T W_o + C^T C = 0} \tag{2.42}$$

To get the balanced form from the linear system in 2.35 there is a state-space transformation $\boldsymbol{\tilde{x} = Tx}$ such that the transformed system gives balance realization which can be written as:

$$\dot{\tilde{\boldsymbol{x}}}(t) = \boldsymbol{\tilde{A}\tilde{x}}(t) + \boldsymbol{\tilde{B}u}(t) \tag{2.43a}$$

$$\boldsymbol{y}(t) = \boldsymbol{\tilde{C}\tilde{x}}(t) + \boldsymbol{Du}(t), \tag{2.43b}$$

where:

$\boldsymbol{\tilde{A} = TAT^{-1}} \in \mathbb{R}^{\boldsymbol{n_x \times n_x}}$
$\boldsymbol{\tilde{B} = TB} \in \mathbb{R}^{\boldsymbol{n_x \times n_u}}$
$\boldsymbol{\tilde{C} = CT^{-1}} \in \mathbb{R}^{\boldsymbol{n_y \times n_x}}$
$\boldsymbol{D} \in \mathbb{R}^{\boldsymbol{n_y \times n_u}}$

The transformed controllability and observability Gramians $\tilde{\boldsymbol{W}}_{\boldsymbol{c}}$ and $\tilde{\boldsymbol{W}}_{\boldsymbol{o}}$ are

$$\tilde{\boldsymbol{W}}_{\boldsymbol{c}} = \boldsymbol{T}\boldsymbol{W}_{\boldsymbol{c}}\boldsymbol{T}^{\boldsymbol{T}} \tag{2.44}$$

$$\tilde{\boldsymbol{W}}_{\boldsymbol{o}} = \boldsymbol{T}^{-\boldsymbol{T}}\boldsymbol{W}_{\boldsymbol{o}}\boldsymbol{T}^{-\mathbf{1}} \tag{2.45}$$

If the system is internally balanced that implies

$$\tilde{\boldsymbol{W}}_{\boldsymbol{c}} = \tilde{\boldsymbol{W}}_{\boldsymbol{o}} = \boldsymbol{\Sigma} = \operatorname{diag}\{\sigma_1, \sigma_2, \ldots, \sigma_{n_r}, \sigma_{n_r+1}, \ldots, \sigma_{n_x}\} \tag{2.46}$$

where the Hankel singular values are order such that $\sigma_1 \geq \sigma_2 \geq \ldots \sigma_{n_r} \geq \sigma_{n_r+1} \geq \ldots \geq \sigma_{n_x}$ implying that the higher the value of σ_i the higher the energy of that state in the system. The states in the balanced form can be divided into two groups. The first group $\boldsymbol{x_r}$ is controllable and observable which is corresponding to the Hankel singular values $\sigma_1, \sigma_2, \ldots, \sigma_{n_r}$,i.e., these states are kept. The second group $\boldsymbol{x_t}$ is uncontrollable and unobservable which is corresponding to the Hankel singular values $\sigma_{n_r+1}, \ldots, \sigma_{n_x}$,i.e., these states can be truncated. However, there are different criteria that determine number of states that can be truncated which is discussed in section 2.5.3. Therefore, the balanced realization in 2.43 can be partitioned as:

$$\begin{bmatrix} \dot{\boldsymbol{x}}_r(t) \\ \dot{\boldsymbol{x}}_t(t) \end{bmatrix} = \begin{bmatrix} \boldsymbol{A_{11}} & \boldsymbol{A_{12}} \\ \boldsymbol{A_{21}} & \boldsymbol{A_{22}} \end{bmatrix} \begin{bmatrix} \boldsymbol{x}_r(t) \\ \boldsymbol{x}_t(t) \end{bmatrix} + \begin{bmatrix} \boldsymbol{B_1} \\ \boldsymbol{B_2} \end{bmatrix} \boldsymbol{u}(t) \tag{2.47a}$$

$$\boldsymbol{y}(t) = \begin{bmatrix} \boldsymbol{C_1} & \boldsymbol{C_2} \end{bmatrix} \begin{bmatrix} \boldsymbol{x}_r(t) \\ \boldsymbol{x}_t(t) \end{bmatrix} + \boldsymbol{D}\boldsymbol{u}(t) \tag{2.47b}$$

Using the Criteria in 2.5.3 the states $\boldsymbol{x_t}$ can be truncated and the reduced order model can be formed:

$$\dot{\boldsymbol{x}}_r(t) = \underbrace{\boldsymbol{A_{11}}}_{\boldsymbol{A}_r} \boldsymbol{x}_r(t) + \underbrace{\boldsymbol{B_1}}_{\boldsymbol{B}_r} \boldsymbol{u}(t) \tag{2.48a}$$

$$\boldsymbol{y}(t) = \underbrace{\boldsymbol{C_1}}_{\boldsymbol{C}_r} \boldsymbol{x}_r(t) + \boldsymbol{D}\boldsymbol{u}(t), \tag{2.48b}$$

where $\boldsymbol{A}_r \in \mathbb{R}^{n_r \times n_r}, \boldsymbol{B}_r \in \mathbb{R}^{n_r \times n_u}, \boldsymbol{C}_r \in \mathbb{R}^{n_y \times n_r}, \boldsymbol{D}_r \in \mathbb{R}^{n_y \times n_u}, n_r \ll n_x$.

2.5.2.2 Matched DC Gain method

The Matched DC Gain (MDCG) method can be used to reduce the order of linear models such that the reduced-order model is close, in some sense, as in section 2.5.3, to the full-

order model. The principle is to alter the remaining states to maintain the DC gain of the system. In general, maintaining the DC gain yields sacrificing accuracy in higher-frequency dynamics. The MDCG depends on transferring the original linear model to the balance realization as is done in BT method in section 2.5.2.1 to get the balanced realization model in 2.43

$$\begin{bmatrix} \dot{\boldsymbol{x}}_r(t) \\ \dot{\boldsymbol{x}}_t(t) \end{bmatrix} = \begin{bmatrix} \boldsymbol{A_{11}} & \boldsymbol{A_{12}} \\ \boldsymbol{A_{21}} & \boldsymbol{A_{22}} \end{bmatrix} \begin{bmatrix} \boldsymbol{x}_r(t) \\ \boldsymbol{x}_t(t) \end{bmatrix} + \begin{bmatrix} \boldsymbol{B_1} \\ \boldsymbol{B_2} \end{bmatrix} \boldsymbol{u}(t) \tag{2.49a}$$

$$\boldsymbol{y}(t) = \begin{bmatrix} \boldsymbol{C_1} & \boldsymbol{C_2} \end{bmatrix} \begin{bmatrix} \boldsymbol{x}_r(t) \\ \boldsymbol{x}_t(t) \end{bmatrix} + \boldsymbol{D}\boldsymbol{u}(t) \tag{2.49b}$$

Then the state-space matrices of the obtained model are recomputed by assuming that x_t converge to the steady state much faster than x_r,i.e, by setting the $\dot{\boldsymbol{x}}_{\boldsymbol{r}}$ to zero [8], two equation are obtained:

$$\dot{\boldsymbol{x}}_r(t) = \boldsymbol{A_{11}}\boldsymbol{x}_r(t) + \boldsymbol{A_{12}}\boldsymbol{x}_t(t) + \boldsymbol{B_1}\boldsymbol{u}(t) \tag{2.50}$$

$$\boldsymbol{x}_t(t) = -\boldsymbol{A_{22}^{-1}}\boldsymbol{A_{21}}\boldsymbol{x}_r(t) - \boldsymbol{A_{22}^{-1}}\boldsymbol{B_2}\boldsymbol{u}(t), \tag{2.51}$$

where $\boldsymbol{A_{22}}$ must be invertable. By inserting equation 2.51 in equations 2.50 and 2.49b, the reduced-order model can be described as

$$\dot{\boldsymbol{x}}_r(t) = \left[\boldsymbol{A_{11}} - \boldsymbol{A_{12}}\boldsymbol{A_{22}^{-1}}\boldsymbol{A_{21}}\right]\boldsymbol{x}_r(t) + \left[\boldsymbol{B_1} - \boldsymbol{A_{12}}\boldsymbol{A_{22}^{-1}}\boldsymbol{B_2}\right]\boldsymbol{u}(t) \tag{2.52a}$$

$$\boldsymbol{y}(t) = \left[\boldsymbol{C_1} - \boldsymbol{C_2}\boldsymbol{A_{22}^{-1}}\boldsymbol{A_{21}}\right]\boldsymbol{x}_r(t) + \left[\boldsymbol{D} - \boldsymbol{C_2}\boldsymbol{A_{22}^{-1}}\boldsymbol{B_2}\right]\boldsymbol{u}(t) \tag{2.52b}$$

To measure how the reduced-order close to the full order model, the criteria in the next section are used.

2.5.3 Choosing of the reduction order criteria

Choosing the order of the reduced model n_r and how the full-order model and reduced-order model are closed is an important issue in model reduction. Two criteria are used

- **Error Bounded:** The reduced-order model achieved by truncating the states that corresponding to smaller Hankel Singular Values(HSVs),i.e., $\sigma_{n_r+1}, \ldots, \sigma_{n_x}$, where n_r ans n_x are reduced order and full order, respectively [21, 4]. However, the error

bounded can be calculated if this condition is fulfilled

$$\sum_{i=1}^{n_r} \left(\sigma_i^2\right)^{1/2} \gg \sum_{i=n_r+1}^{n_x} \left(\sigma_i^2\right)^{1/2} \tag{2.53}$$

The error bounded is given:

$$E_\infty = \|\boldsymbol{E}_k(s)\|_{L_\infty} = \|\boldsymbol{G}(s) - \boldsymbol{G}_r(s)\|_{L_\infty} \leq 2\left(\sigma_{n_r+1} + \cdots + \sigma_{n_x}\right) \leq \epsilon, \tag{2.54}$$

where

$\boldsymbol{G}(s) = \boldsymbol{C}(s\boldsymbol{I} - \boldsymbol{A})^{-1}\boldsymbol{B} + \boldsymbol{D}$ -the transfer function of full-order model

$\boldsymbol{G}(s) = \boldsymbol{C_r}(s\boldsymbol{I} - \boldsymbol{A_r})^{-1}\boldsymbol{B_r} + \boldsymbol{D}$-the transfer function of reduced-order model

ϵ-the desired accuracy.

- **Root Mean Square Error:** Root Mean Square Error (RMSE) is a way to measure the error between the states of the full-order model and the reduced-order model. The states data can be obtained by simulation using different inputs. Then the output data is normalized,i.e., the data has mean 0 and standard deviation 1. RMSE can be formulated [17] as:

$$\Phi_r = \sqrt{\frac{1}{N}\sum_{n=1}^{N} |\boldsymbol{x}_{f_n} - \boldsymbol{x}_{r_n}|^2}, \tag{2.55}$$

where Φ_r is Root Mean Square Error, $\boldsymbol{x}_{f_n}$ is state's data of full-order model, $\boldsymbol{x}_{r_n}$ is state's data of reduced-order model, and N is number of observations.

2.6 Model Predictive Control

Model Predictive Control (MPC) utilizes the model of a system to find optimal control by minimizing an objective function in a receding horizon manner. MPC uses the model to predict the output at a finite-horizon. The MPC principle is solving an online open-loop optimization problem where the system dynamics is used as a constraint with the constraints on states and inputs. This solving is done at each time T_s step by using the current state of our system as initial values. Then, implementing the first control action to the plant. Finally, using receding horizon strategy by moving the horizon one step forward and repeat the procedure [5, 7]. The principle of MPC shows in fig 2.6 which was inspired from [20]. There are two reasons for using a finite horizon instead of an infinite horizon. Firstly, allowing real-time solution and secondly giving the ability to predicate again after

each time step.

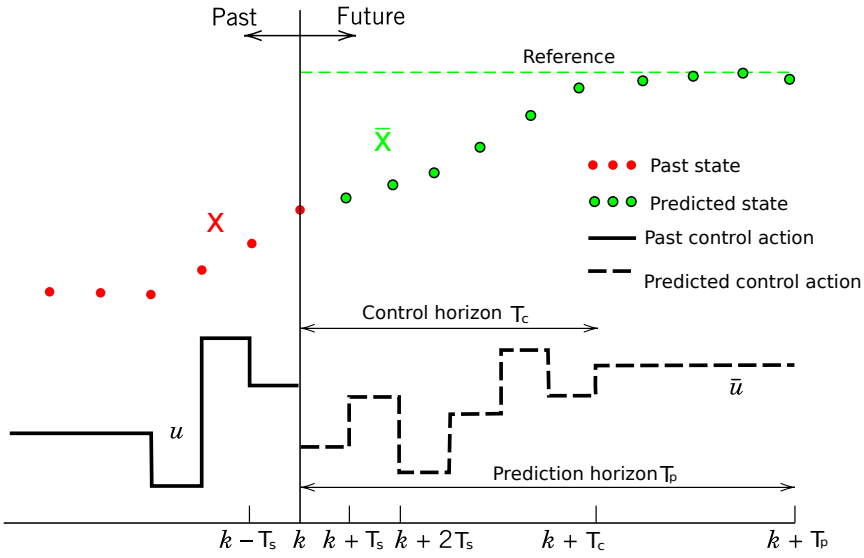

Figure 2.6: The principle of the MPC.

The are advantages of MPC compared to other types of controller:

- MPC can handle Multi-Input Multi-Output (MIMO) systems.
- MPC can handle constraints on states and inputs. Constraints can be either physical limitations of, e.g., the actuators, such as limits of the pitch angle and generator torque, or artificial constraints, such as the rate of change of the pitch angle must be within some limits to prevent the fatigue that could cause to damage [10].
- Moreover, MPC has preview capability, which is similar to feed-forward control. That is why it gets previous information about future trajectory to improve controller performance.

To run MPC faster, some methods can be used, such as model order reduction, shorter prediction horizon T_p, shorter control horizon T_c and reduced number of constraints are the most efficient methods that speed up MPC and reduces the complexity.
Achieving a real-time feasible solution of the MPC optimization problem is the primary goal of using MPC. This is related to the convexity of the optimization problems, where the

convex optimization problem reduces the computational time comparing to the non-convex optimization problem. The optimal local solution for the convex problems is the optimal global solution; this is not the case for the non-convex problems, since the non-convex problems have many local optimal points. In general, all nonlinear MPC (NMPC) is a non-convex optimization problem. In contrast, some of the linear MPC is a convex optimization problem, i.e., the linear MPC is faster than NMPC. However, in this thesis, the linear MPC gives a non-convex problem since we have a non-convex objective function, but it still reduces the computational time. The following presents how the NMPC and linear optimization problems are formulated.

2.6.1 Formulation of the NMPC optimization problem

NMPC optimization problems can be formulated as minimizing an objective function subject to $nonlinear$ system dynamics and constraint on states and inputs as follows [5]:

$$\begin{aligned} \min_{x,z,u} J(z) = & \sum_{t=0}^{N-1} L(x_i, z_i, u_i) + E(x_N) \\ \text{s.t.} \quad & x_{i+1} = f(x_i, z_i, u_i) \\ & x_0 - \bar{x}_0 = 0 \\ & g(x_i, z_i, u_i) = 0 \\ & h(x_i, z_i, u_i) \leq 0 \\ & r\left(x_N\right) \leq 0, \end{aligned} \tag{2.56}$$

where $x_i \in \mathbb{R}^{n_x}$ is the differential state, $z_i \in \mathbb{R}^{n_z}$ the algebraic state, $u_i \in \mathbb{R}^{n_u}$ is the control, $E(x_N)$ is a cost on the final states deviation from a reference, $g(x_i, z_i, u_i)$ is the equality constraint and $h(x_i, z_i, u_i)$ is the inequality constraints. Functions $f \in \mathbb{R}^{n_x}$ and $g \in \mathbb{R}^{n_z}$ are assumed twice differentiable. The state vector is $x = [x_0^T, x_1^T \ldots, x_{N-1}^T, x_N^T]^T$, the algebraic vector is $z = [z_0^T, z_1^T \ldots, z_{N-1}^T]^T$ and the input vector
$u = [u_0^T, u_1^T \ldots, u_{N-1}^T]^T$.

2.6.2 Formulation of the linear MPC optimization problem

Linear MPC optimization problem can be formulated as minimizing an objective function subject to $linear$ system dynamics and constraint on states and inputs as follows [5]:

$$\begin{aligned} \min_{x,z,u} J(z) &= \sum_{t=0}^{N-1} L(x_i, z_i, u_i) + E(x_N) \\ \text{s.t.} \quad & x_{i+1} = Ax_i + Bu_i \\ & x_0 - \bar{x}_0 = 0 \\ & g(x_i, z_i, u_i) = 0 \\ & h(x_i, z_i, u_i) \leq 0 \\ & r\left(x_N\right) \leq 0, \end{aligned} \tag{2.57}$$

2.6.3 MPC design parameters

Choosing parameter values is important for both the controller performance and the computational complexity of the MPC optimization. The parameters that should be designed are sample time T_s, prediction horizon T_p, control horizon T_c, constraints and weights. T_s should not be too big or too small. If T_s is too big, the MPC will not be able to respond to the disturbances quickly. In contrast, if T_s is too small, the MPC will be too aggressive to the disturbances. The prediction horizon T_p should be chosen to satisfy the significant system dynamics. Moreover, increasing the control horizon T_c gives a better prediction, but this leads to increasing the computational time. However, T_c can be equal to the prediction horizon, but the recommendation to be (10-20)% of the prediction horizon. Due to physical limitations, constraints must be used. The recommendation is to use hard constraints on inputs and soft constraints on the output to avoid the conflicts, which will lead to an unfeasible optimal solution. Weights on different terms in objective function choose depending on which term is more important to us than others.

2.6.4 Direct collocation

To transform Optimal Control Program (OCP) as in 2.56 and 2.57 into a Nonlinear Program (NLP), either a collocation method (indirect and direct collocation), or a shooting-based methods (direct single shooting and direct multiple shooting) are used. Libraries like CasADi can easily solve those methods. In this thesis, the direct collocation is used. The direct collocation discretized controls and states in NLP by approximating all of the trajectory as polynomials [5]. Polynomials are used because they represent by a finite number of coefficients, and it is easy to compute integrals and derivatives of polynomials.

The algorithm of using direct collocation is presented in [5] where the states on the grid points are denote by $s_k \approx x(t_k)$ and a parameterization of the controls is chosen as constant or piecewise polynomials, with control parameters q_k which gives on each interval a function $u_k(t;q)$ the control parameters. On each collocation interval a set of m collection points is chosen and trajectory is approximated by a polynomial $p_k(t;v_k)$ with coefficient vector v_k. The following conditions are added to the NLP to enforce the dynamics at the collocation points [5]:

$$s_k = p_k(t_k; v_k) \tag{2.58a}$$

$$f(p_k(t_k^1; v_k), u_k(t_k^1; q_k)) = p_k(t_k^1; v) \tag{2.58b}$$

$$\vdots$$

$$f(p_k(t_k^m; v_k), u_k(t_k^m; q_k)) = p_k(t_k^m; v) \tag{2.58c}$$

By recapping the system by the vector $c_k(s_k, v_k, q_k) = 0$. Moreover, it needs continuity across interval, i.e. adding the constraints $p_k(t_{k+1}; v_k)s_{k+1} = 0$. By approximating the integrals cost contribution:

$$\int_{t_k}^{t_{k+1}} L(x,u)dt \tag{2.59}$$

by a quadrature formula. The NLP can be formulated as [5]:

$$\begin{aligned}
\min_{s,v,q} \quad & \sum_{k=0}^{N-1} l_k(s_k, v_k, q_k) + E(s_N) \\
\text{s.t.} \quad & s_0 - x_0 = 0, && && \text{(initial value)} \\
& c_k(s_k, v_k, q_k) = 0, && k = 0, ..., N-1, && \text{(collocation conditions)} \\
& p_k(t_{k+1}; v_k)s_{k+1} = 0, && k = 0, ..., N-1, && \text{(continuity across intervals)} \\
& h(s_k, q_k) \leqslant 0, && k = 0, ..., N-1, && \text{(discretized path constraints)} \\
& r(s_N) \leqslant 0, && && \text{(terminal constraints)}
\end{aligned} \tag{2.60}$$

where $E(s_N)$ is a cost on the final states deviation from a reference.

2.6.5 CasADi

CasADi is a *symbolic* framework for Algorithmic Differentiation (AD) using a syntax from Computer Algebra Systems (CAS) [2]. CasADi is an open-source tool uses for optimization, and it allows to structure symbolic codes. These codes can then be easily differentiated. To solve NLP as in 2.60, the nonlinear solver *ipopt* is used.

Chapter 3

Methodology

This chapter gives an explanation of how the data was obtained and the methods are applied. It explains how the wind field is created, which model reduction methods are used and how the models are reduced, and finally, the MPC with linear (full-order and reduced-order) and nonlinear model is covered.

3.1 Wind profile

Wind speed feeds into the model as described in section 2.4.6. Both constant wind speed ($14\,m.s^{-1}$) and turbulent wind speeds with mean wind speed ($14\,m.s^{-1}$) are used. In some scenarios, the turbulent wind speeds are used by assuming that we have perfect knowledge about the wind speed. For some scenarios, the constant wind speed is used by supposing that we do not have full knowledge about the wind speed. However, the turbulent wind speeds are created using the code $gen\_windfield$ in [1] where the data used to create is: mean wind speed (U_0=14 $m.s^{-1}$), turbulence intensity (T_i=0.1), grid resolution (d=15 m), the length of the wind field (L_x=1e3 m), the width of the wind field (L_y=1.5e3 m), the maximum simulation time (T_w=200 s) with 1 s time step, and the wind shear exponent α=0.15. In general, the wind speed for the top rotors is higher than the lower rotors. Fig. 3.1 shows the wind speed profile for the four single turbines $R1$, $R2$, $R3$, and $R4$.

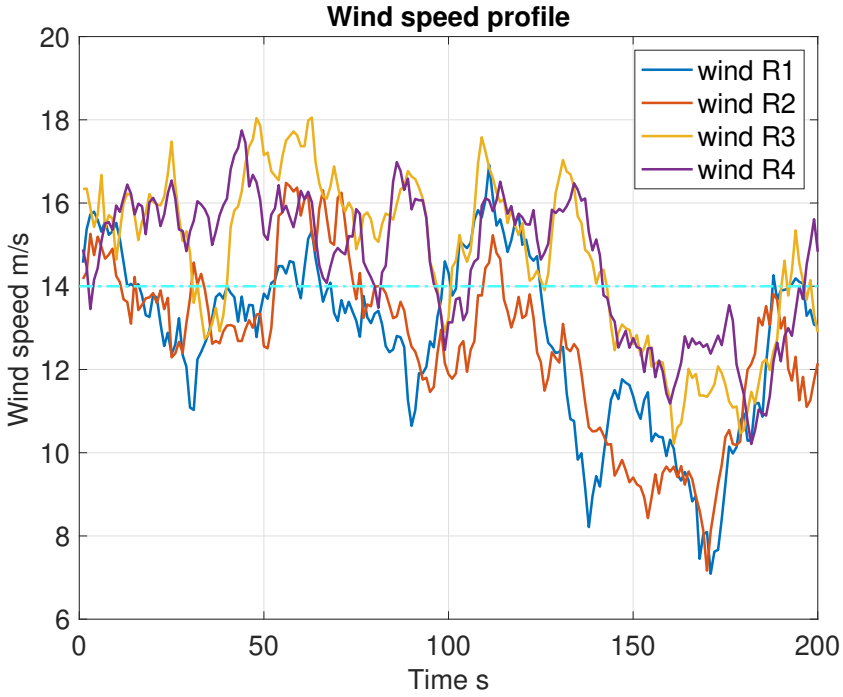

Figure 3.1: Wind speed profile for the four-rotor $R1$, $R2$, $R3$, and $R4$

3.2 C_P and C_T

The nonlinear polynomial method, as described in section 2.2, utilized to calculate the power coefficients and the thrust coefficients. The numerical experiments using Casadi showed that the nonlinear polynomial method is faster in the optimization than the interpolation method.

3.3 RMSE calculation

RMSE is used to measure the accuracy of reduced-order as in section 2.5.3 where the data is normalized. It is obtained from the simulation of models. Moreover, RMSE is utilized to measure the error between the power reference (20 MW) and actual power production. The RMSE is applied to measure how the loads on the tower reduced for different scenarios. RMSE for power and loads can be calculated as:

$$\Phi_p = \sqrt{\frac{1}{N}\sum_{n=1}^{N} |20MW - P_{tot_n}|^2} \tag{3.1}$$

$$\Phi_l = \sqrt{\frac{1}{N}\sum_{n=1}^{N} \left| \boldsymbol{L}_{tow_{ref_n}} - \boldsymbol{L}_{tow_n} \right|^2}, \tag{3.2}$$

where Φ_p and Φ_l are the RMSE of power production and loads on the tower structure, respectively. P_{tot_n} and $\boldsymbol{L}_{tow_n}$ are the total power production of a 4RT at the observation n and loads on tower at the observation n, respectively. N is the number of observations. $\boldsymbol{L}_{tow_{ref_n}}$ is the reference load. The reference load obtained by removing the load term from the objective function. Then the optimization is run. Here we have two different reference loads. One reference load obtained when the turbulent wind is used, and another reference load is obtained in case of the constant wind speed. The data used to calculate RMSE load is normalized, i.e., data has mean 0 and standard deviation 1. whereas, the data for power is not normalized, and the reference is 20 MW.

3.4 Reduced-model

The nonlinear four-rotor model is linearized using the Taylor series expansion. The linearization of nonlinear four-rotor is done around different operating points for different wind speeds as a parameter, where the values of the parameter are between (2 $m.s^{-1}$ and 25 $m.s^{-1}$). However, Not all linearized models were used. To ensure the real-time optimization, the models of the tower and 4RT are reduced using Balanced Truncation (BT) and Matched DC Gain (MDCG) methods. The linearized model of the 4RT is reduced from 20 to 4 states using MDCG. The reduced-order model must be close to the full-order model. The closeness is measured by Root Mean Square Error (RMSE). The RMSE is calculated of the data obtained by simulation of the full-order and the reduced-order models using 600 different inputs. Nevertheless, the 4RT model could not be reduced using BT without missing some states' accuracy. Therefore, the reduction using BT was not included for 4RT.

The linear tower model was reduced from 20 to 11 states using MDCG. Moreover, the tower model could not be reduced to less than 17 states using BT without increasing the RMSE, i.e., reducing the accuracy. The RMSE calculated for the tower models by getting the response of the models by simulation, where 600 different inputs were used for full-order and reduced-order models.

3.5 MPC

The main goal of reduced-order models is to allow the MPC to run in real-time. The real-time for MPC refers to finding the optimal solution in less than T/N seconds, where T is the prediction horizon, and N is the number of intervals. In this thesis, $T = 10$ seconds

and $N = 10$ for linear MPC. Which means the optimal solution must be found in less than one second. The following facts and assumptions for using MPC are considered:

- MPC has two inputs (power P_{ref} and pitch angle β_{ref}) for each of 4RT.
- There will be no feedback from the plant, i.e., the initial state of the optimization will not be updated.
- Time step for linear MPC is one second. The time step for NMPC is larger, and it differs from scenario to another.
- The weight on the power term is larger in case of using the turbulent wind speeds. The choice was to give a better power tracking when the low wind speeds meet. On the other hand, the weight on the power term is lower in the case of the constant wind speed. Note that the weights on power and load are the same in all scenarios where constant wind speed is used (for both linear MPC and NMPC).

Different scenarios for optimization are used. Turbulent wind speeds as in fig 3.1 and constant wind speed 14 $m.s^{-1}$ is used for NMPC. However, only constant wind speed is applied for linear MPC. There was a plan to utilize turbulent wind speeds for linear MPC. That could be done by interpolation of the linearized model at different parameter values p. The interpolation could not be achieved due to time restriction.

Here is a summary of the different scenarios that are used in this thesis.

- Firstly, the Full-Order Nonlinear (FON) of the Four-Rotor Turbine (4RT) and Full-Order Tower (FOT) models were implemented (both turbulent wind speeds and constant wind speed).
- Secondly, the Full-Order Nonlinear (FON) of 4RT model and Reduced-Order Tower (ROT) model (reduced to 11 states using MDCG) was implemented (both turbulent wind speeds and constant wind speed). However, the ROT model using BT was not implemented in the case of NMPC. The BT method gave the same results as MDCG, where both methods could not run in real-time optimization.
- Thirdly, the Full-Order Linearized (FOL) of 4RT is implemented with both the Full-Order Tower (FOT) and the Reduced-Order Tower (ROT) models.
- Finally, the Reduced-Order Linearized (ROL) of 4RT and Reduced-Order Tower (ROT) models are used.

In all scenarios, the initial states is: $\boldsymbol{x}_0 = [1.19, 116, 0.003, 31300, 5, 1.19, 116, 0.003, 31300, 5, 1.19, 116, 0.003, 31300, 5, 1.19, 116, 0.003, 31300, 5, \text{zeros}(20, 1)^T]^T$.

The direct collocation method was chosen to transfer the Optimal Control Problem (OCP) into a finite-dimensional Nonlinear Program (NLP). The order of the collocation polynomial is four. Moreover, Casadi package included in Matlab, and the solver $ipopt$ for NLP used.

3.6 Control objective for optimization

The main objective is to maximize or track the power (20 MW) and minimize the load on the tower. Both power and load are included in objective function as in equation 2.31. However, there are limitations on power, rotor speed, and generator speed to keep them below some values to keep the turbine from unsafe operations under high wind conditions. Therefore, the constraints on the generator speed ω, the rotor speed Ω, and the generator torque M_{gen} applied as in table 3.1. The constraint on inputs (pitch angle β_{ref} and power reference P_{ref}) for individual turbine are also applied. β_{ref} restricted between 0° and 20°, where P_{ref} is restricted between 0 MW and 5 MW. Moreover, the constraints on the actual power production for each single turbine is used to keep the maximum power 5 MW, i.e., the maximum total power is 20 MW, which will be the power reference for the objective function. Table 3.1 gives the rated values of states and inputs. The results for all optimization scenarios will satisfy the rated values for states and power.

Rated values	
Rated Power	5.296 MW
Rated Generator Speed	122.9 $r.s^{-1}$
Rated Rotor Speed	1.267 $r.s^{-1}$
Maximum Generator Torque	4.74e+5 $N.m$
Maximum Pitch Angle	90°
Maximum Pitch Angle (input)	20°

Table 3.1: Rated values of states, inputs and power.

We have two terms in the objective function, one of them represents the power tracking, and the other represents the loads on the tower structure. The weights on two terms determine which of them are more important to us than another. We tried to choose the weights on both terms to keep a proper power tracking, and simultaneously time to reduce the loads on the tower. We could have perfect power tracking, but this means that we sacrifice the loads reduction, which could lead to damage to the tower structure.

Table 3.2 summarises all scenarios that will be tested in this thesis with their different conditions. This will help to follow our results in the next section. The table contains the short acronym names for each model, the type of model nonlinear or linear, the reduction method, the time step, and the wind speed type (turbulent or constant). The acronym names for each model can be described as follows:

- FON of 4RT & FOT represents Full-Order Nonlinear of Four-Rotor Turbine and Full-Order Tower models.
- FON of 4RT & ROT represents Full-Order Nonlinear of Four-Rotor Turbine and Reduced-Order Tower models.
- FOL of 4RT & FOT represents Full-Order Linearized of Four-Rotor Turbine and Full-Order Tower models.
- FOL of 4RT & ROT represents Full-Order Linearized of Four-Rotor Turbine and Reduced-Order Tower models.
- ROL of 4RT & ROT represents Reduced-Order Linearized of Four-Rotor Turbine and Reduced-Order Tower models.

The short acronym names for each reduction method can be described as follows:

- BT represents Balanced Truncation.
- MDCG represents Matched DC Gain.

All scenarios with their conditions				
Model	Nonlinear/ linear	Model reduction turbine/tower	Time step	Turbulent/ constant wind
FON of 4RT &FOT	Nonlinear	-	3s	Turbulent
FON of 4RT &FOT	Nonlinear	-	2s	Constant
FON of 4RT &ROT	Nonlinear	- & MDCG	2s	Turbulent
FON of 4RT &ROT	Nonlinear	- & MDCG	2s	Constant
FOL of 4RT &FOT	Linear	-	1s	Constant
FOL of 4RT &ROT	Linear	- & BT	1s	Constant
FOL of 4RT &ROT	Linear	- &MDCG	1s	Constant
ROL of 4RT &ROT	Linear	MDCG &BT	1s	Constant
ROL of 4RT &ROT	Linear	MDCG &MDCG	1s	Constant

Table 3.2: All scenarios that will be implemented in this thesis with their conditions, where in model reduction column, the 4RT and the tower models were reduced separately.

Chapter 4

Analysis

This chapter gives the results of the thesis. Firstly, the performance of the full-order model is compared to the reduced-order model of both tower and 4RT, where there is no optimization. Secondly, the optimization is done for the full-order model for the nonlinear 4RT and tower. This shows the response of NMPC with turbulent and constant wind speeds. Thirdly, the results of NMPC with reduced-order of tower model is presented. Finally, the response of linear MPC of linearized 4RT is presented. Both full-order and the reduced-order of linear MPC are implemented with constant wind speed.

4.1 Simulation of model reduction

To measure how close the reduced-order model to the full-order model, simulation is done on both models by using the Matlab solver $ode15s$. This was necessary before running optimization. The following is a brief of how the model is reduced, and how the error between the reduced-order and the full-order model is measured.

4.1.1 Reduction-order of four-rotor turbine

The linearized four-rotor turbine (4RT) model was reduced from 20 to 4 states using matched DC gain (MDCG), where wind speed 14 $m.s^{-1}$ is used as a linearized parameter. Then, the linearized model was reduced with the balanced truncation (BT) method, but the RMSEs were high,i.e., the accuracy was low. Therefore, the results are not presented. Table 4.1 gives root mean square error (RMSE) and the accuracy in percentage, where the RMSE calculated between the response of the full-order and the response of reduced-order. The simulation performed to get a response by implementing 600 different inputs. The highest RMSE is 0.0085,i.e, the lowest accuracy is 99.14% corresponding to

state x_8. Therefore, all RMSE gave very low values, i.e., the accuracy is very high. Thus, the reduced-order model represents the full-order model with sufficient accuracy.

Error in reduced 4RT model		
States	RMSE	Accuracy %
x_1	0.0011	99.89
x_2	0.0012	99.87
x_3	0.0067	99.31
x_4	0.0009	99.91
x_5	0.0027	99.72
x_6	0.0015	99.84
x_7	0.0017	99.82
x_8	0.0085	99.14
x_9	0.0012	99.87
x_{10}	0.0028	99.71
x_{11}	0.0009	99.91
x_{12}	0.0009	99.91
x_{13}	0.0052	99.47
x_{14}	0.0007	99.92
x_{15}	0.0017	99.82
x_{16}	0.0011	99.89
x_{17}	0.0011	99.89
x_{18}	0.0071	99.28
x_{19}	0.0008	99.91
x_{20}	0.0015	99.84

Table 4.1: Error in the response of the reduced-order model compared to the full-order model for 4RT using MDCG method.

4.1.2 Reduction-order of linear tower model

Two methods are used to reduce the order of the model. Using BT reduced the model from 20 to 17 states while keeping RMSE at the acceptable level, where the lowest RMSE is 0.0567,i.e., the accuracy is 94.33 % as in table 4.2. Using MDCG reduced the model from 20 to 11 states with preservation of the RMSEs for all states at an acceptable level. Table 4.2 shows that lowest RMSE values is 0.0388,i.e., accuracy 96.11 % corresponding to state x_{11}. The reduced-order model is well representing of the full-order model for both methods.

Error in reduced tower model				
States	RMSE BT	Accuracy %	RMSE MDCG	Accuracy %
x_1	0.0001	99.98	0.0006	99.93
x_2	0.00007	99.99	0.0003	99.96
x_3	0.0004	99.96	0.0018	99.81
x_4	0.0004	99.95	0.0019	99.8
x_5	0.0004	99.96	0.0016	99.84
x_6	0.0005	99.95	0.002	99.79
x_7	0.0022	99.77	0.0022	99.78
x_8	0.0023	99.77	0.0019	99.8
x_9	0.0013	99.87	0.002	99.79
x_{10}	0.0013	99.87	0.002	99.79
x_{11}	0.0025	99.75	0.0388	96.11
x_{12}	0.0015	99.85	0.0195	98.04
x_{13}	0.0017	99.83	0.0057	99.42
x_{14}	0.0009	99.911	0.0052	99.47
x_{15}	0.0013	99.87	0.0052	99.47
x_{16}	0.0038	99.62	0.0089	99.1
x_{17}	0.0567	94.33	0.0523	94.76
x_{18}	0.056	94.39	0.0367	96.32
x_{19}	0.0337	96.63	0.0056	99.43
x_{20}	0.0336	96.64	0.0056	99.43

Table 4.2: Error in the response of the reduced-order model compared to the full-order model for tower using BT and MDCG.

To avoid high numbers of plots, the response of the 4RT is not included. The response of the full-order and reduced-order for the tower model using MDCG is plotted. The plots of the first 10 states show in figures 4.1, where figures 4.2 show the last 10 states. The figures show that both the full-order and reduced-order models are similar.

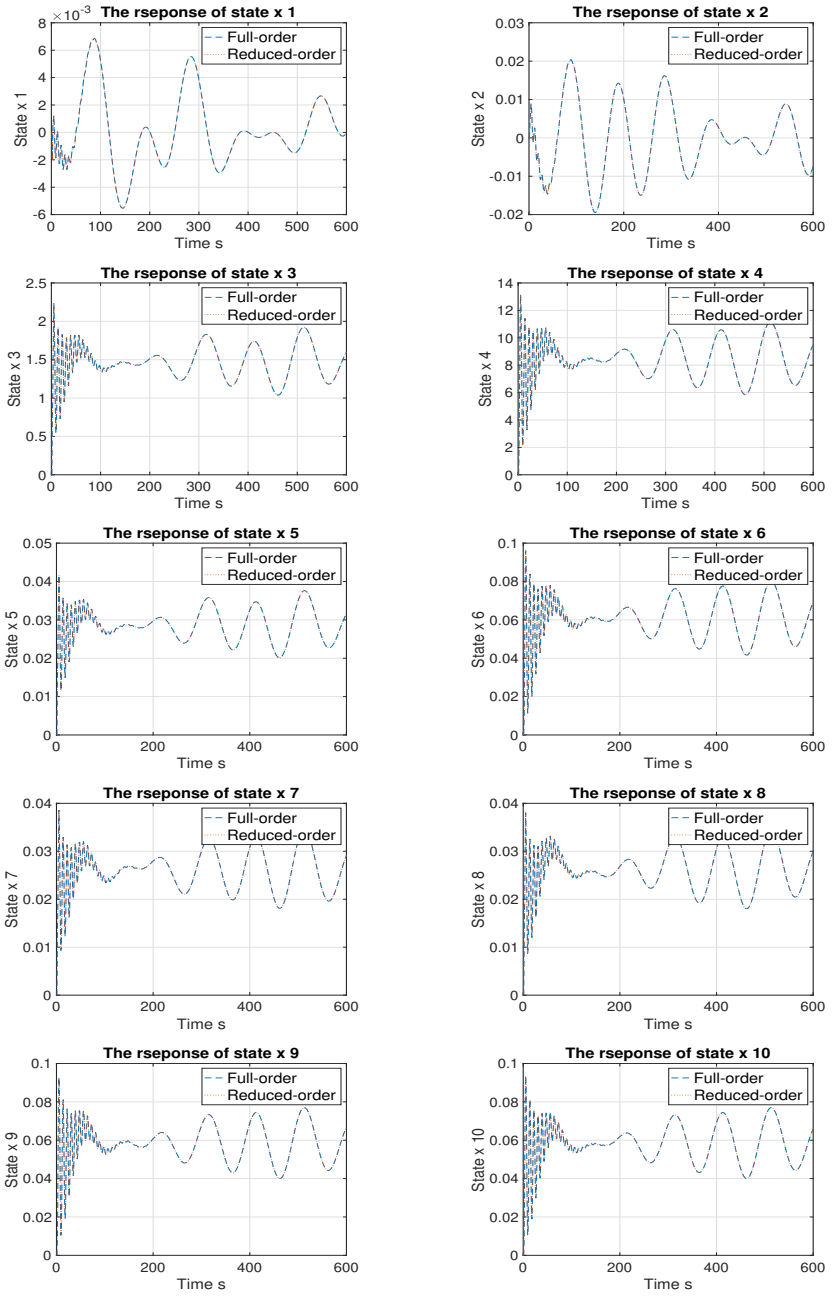

Figure 4.1: The response of the first 10 states of full-order and reduced-order for tower model using MDCG.

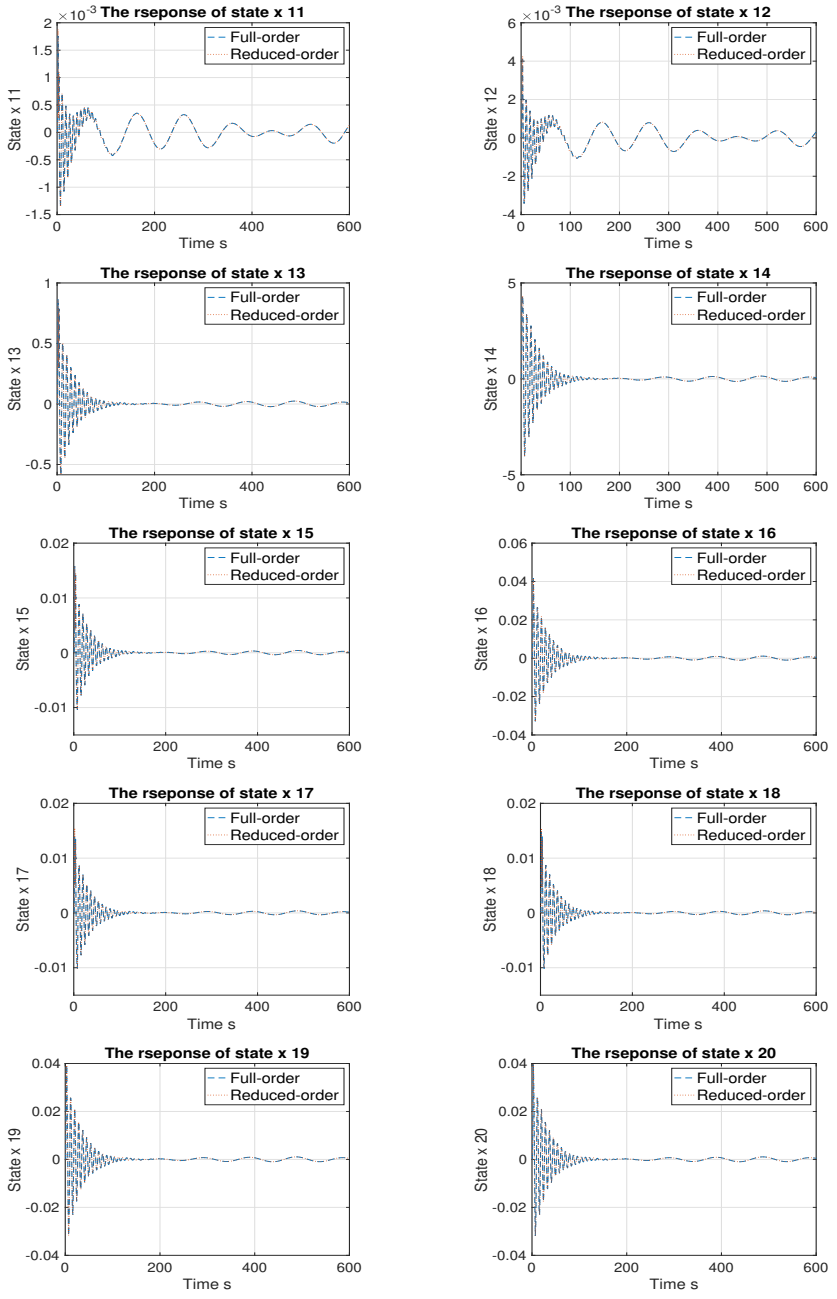

Figure 4.2: The response of the last 10 states of full-order and reduced-order for tower model using MDCG.

4.2 NMPC of four-rotor turbine

This section presents the results of the implementation of NMPC as defined in section 2.6.1,i.e., the nonlinear model of the 4RT. Firstly, the turbulent wind speeds are applied to the nonlinear 4RT model (with full-order tower (FOT) and reduced-order tower (ROT)). Here the weight on the power term in the objective is increased since the wind speed in some time steps is too low,i.e., the wind speed is below the rated wind speed. Then constant wind speed (14 $m.s^{-1}$) is used for the nonlinear 4RT model (with full-order tower (FOT) and reduced-order tower (ROT)). In all scenarios, the actual total power and the actual power of each single turbine, generator speeds, and generator torques are plotted from the second time step, where the response for the first step corresponds to the initial states. The reason for this is that we wanted to show how the response changes from the second step. The result for both the full-order and reduced-order tower models are shown in the following sections.

4.2.1 Full-order nonlinear of four-rotor turbine and full-order tower models

The time step of the wind is one second, whereas the time step of NMPC in this scenario is three seconds. Accordingly, we had to do interpolation by choosing one of the wind speeds every three seconds. Fig 4.3 shows the response of the NMPC using turbulent wind speeds that are defined in fig. 3.1. The model responds to the jumps in the inputs, but it leads to poor power tracking. The turbine is pitching when the low wind speed meets and increases the rotor speed; then, the generator speed increases. This leads to an increase in actual power. The model still can not track the power correctly in some time steps. In other words, if the wind speed is below the rated wind speed as discussed in section 2.3, that leads to the turbine to work in the region I or the region II of the ideal power curve. Thus, the turbine can not reach the rated power (5 MW). Further, the computational time was heavy; meaning could not run in real-time optimization, i.e., the optimal solution was found in more than three seconds. Later, we will provide the RMSE between the actual and desired power.

The loads on the tower's structure compared to the reference loads can be seen in fig 4.4. Note that the reference load is obtained by running optimization with only the power term in case of turbulent wind speeds. Nevertheless, the load minimizing is not promising. There are three reasons for this. Firstly, we chose a large NMPC's time step (three seconds) to reduce the computational time. As we discussed in section 2.6.3, a large time step leads that the model does not respond to the disturbances quickly. Secondly, we increased the weight on the power term in the objective function. Lastly, high wind speeds in some time

steps lead to increase the loads. Those reasons lead to weak load reduction. Later, we will provide the RMSE between the actual and reference loads.

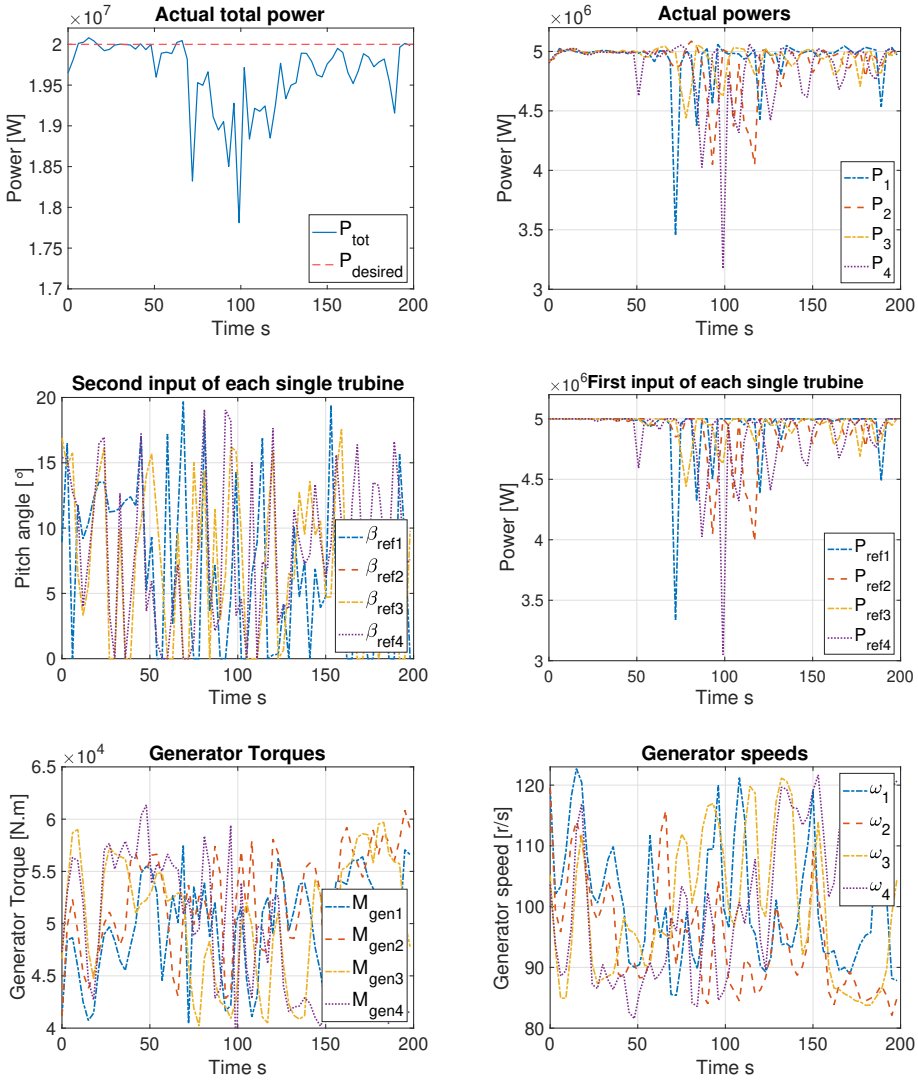

Figure 4.3: The response of NMPC of full-order nonlinear model (FON) of 4RT and full-order tower (FOT) models with turbulent wind speeds.

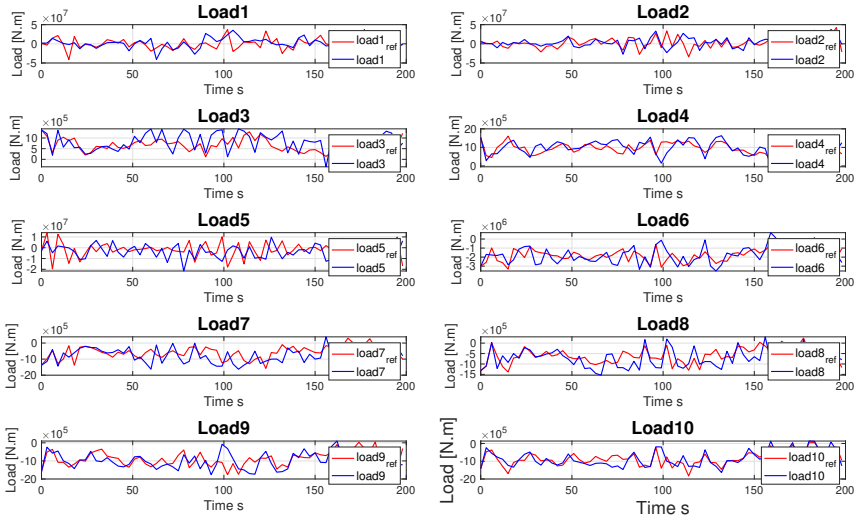

Figure 4.4: Loads on the tower compared to the reference load when NMPC implemented of the full-order nonlinear (FON) of 4RT model and full-order tower (FOT) model (turbulent wind speeds).

Fig. 4.5 presents the response of the NMPC of full-order nonlinear (FON) of the 4RT model and full-order tower model using constant wind speed. The time step for NMPC is two seconds in this scenario. There are many jumps in pitch, which leads to the jumps in generator speed and torque. Then instability in power production. Large-time steps in NMPC results in those jumps and instability. However, an acceptable power tracking is achieved.

Fig. 4.6 presents the loads on the tower in case of constant wind speed. The jumps are removed compared to the reference loads and good load reduction is achieved. Note that the reference load obtained by running the optimization with only the power term in case of constant wind speed. Load reduction in this scenario is better than with turbulent wind speeds.

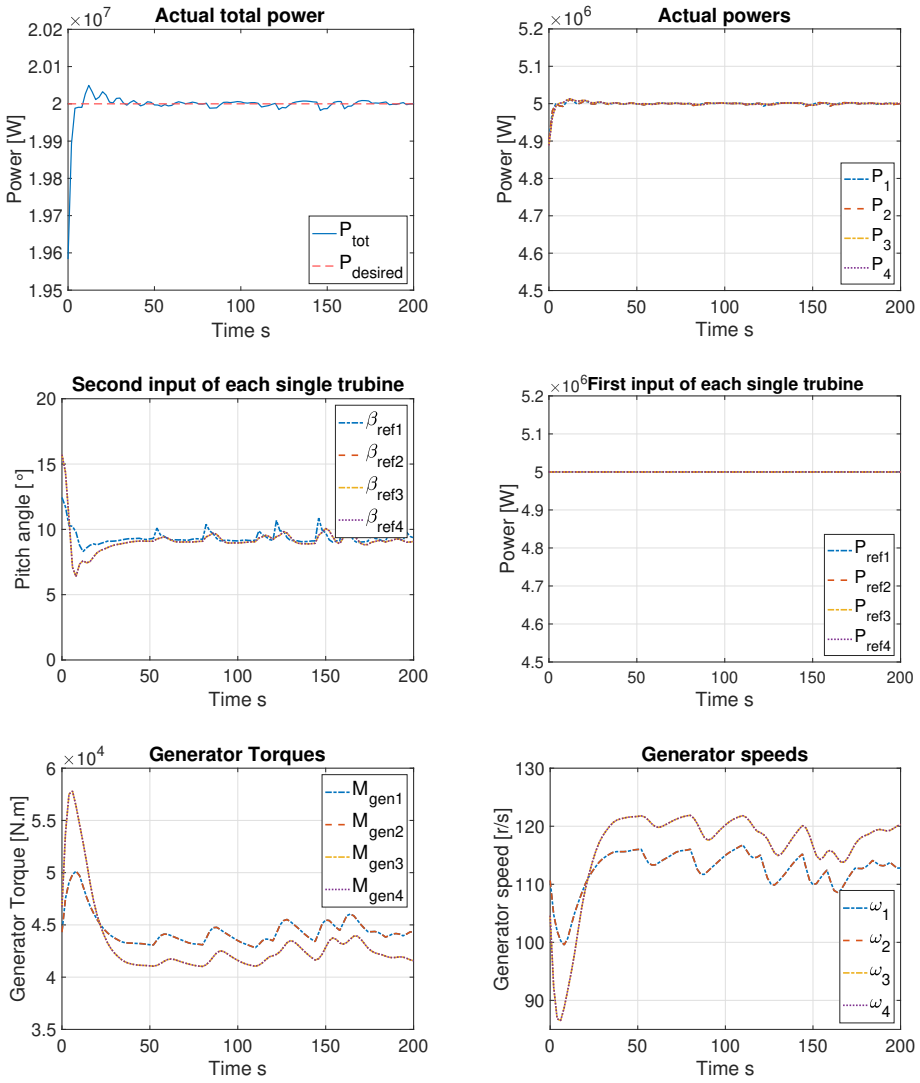

Figure 4.5: The response of NMPC of FON of 4RT and FOT models with constant wind speed.

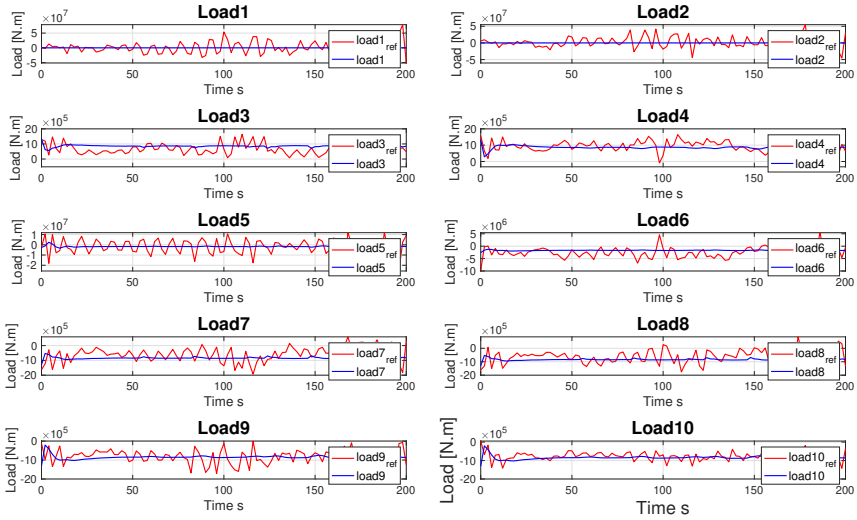

Figure 4.6: Loads on the tower compared to the reference load when NMPC implemented of the FON of 4RT and FOT models with constant wind speed.

4.2.2 Full-order nonlinear of 4RT and reduced-order tower models

Fig. 4.7 shows the response of the NMPC of Full-order nonlinear (FON) of 4RT and reduced-order tower (ROT) using the MDCG method, where the turbulent wind speeds are applied. The tower model reduced from 20 to 11 states. The computational time reduced to half comparing to the NMPC when the full-order tower (FOT) model is used. However, it suffered from long computational time, meaning it could not run in real-time. The power tracking is better than the NMPC with the full-order tower (FOT) model. The MPC's time step is (two seconds) in this scenario, where it was three seconds in the previous scenario. A shorter time step gives a better power tracking. Moreover, the interpolation for wind speed is done for both scenarios. Here we chose one wind speed every two seconds. Whereas, in the previous scenario, we chose one wind speed every three seconds. This interpolation of wind speed also leads to different behavior.

The loads on the tower are shown in fig. 4.8, where turbulent wind speeds are used. Using a larger weight on the power term and different wind speeds result in no promising load reduction.

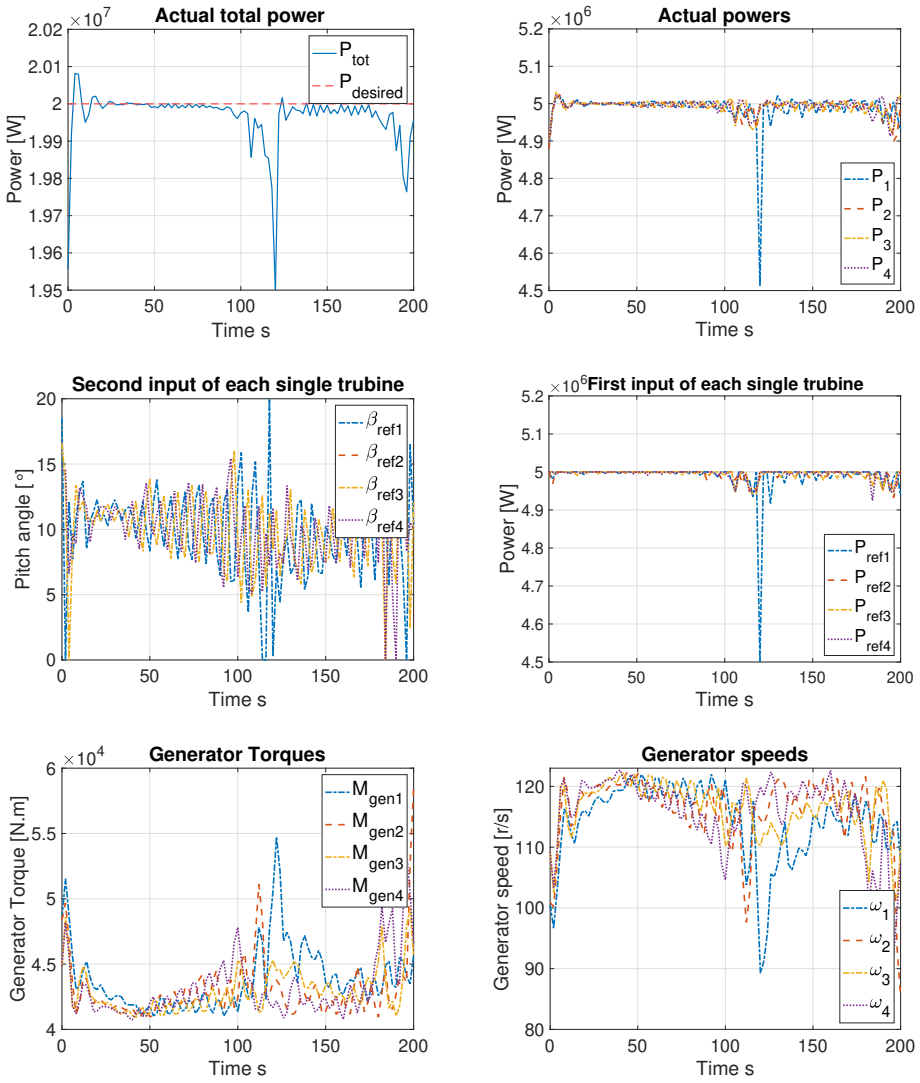

Figure 4.7: The response of NMPC of the FON of 4RT model and reduced-order tower (ROT) model with MDCG (turbulent wind speeds).

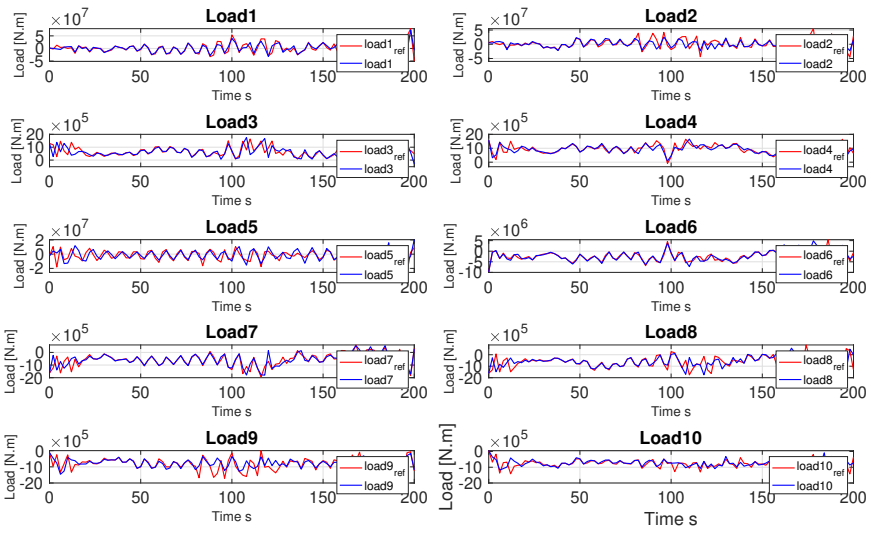

Figure 4.8: Loads on the tower compared to the reference load when NMPC implemented of the FON of 4RT model and reduced-order tower (ROT) model with MDCG (turbulent wind speeds).

Fig. 4.9 contains the response of the NMPC of full-order nonlinear 4RT and reduced-order model of the tower using the matched gain method, where the constant wind speed is used. The power tracking is close to the scenario of the NMPC full-order tower model. One advantage is that the computational time reduced to half compared to that scenario. Nevertheless, it could not run in real-time.
Fig. 4.10 gives the loads on the tower. The loads reduced, and the jumps removed compared to the reference.

The NMPC for all scenarios could not achieve the real-time optimization. Moreover, the power tracking was not perfect due to using a large time step and we decided to use the MPC outputs and not create a feedback plant since feedback resulted in numerical issues. Moreover, the NMPC could not run in real-time. Therefore, the linearized 4RT model is used in the next section.

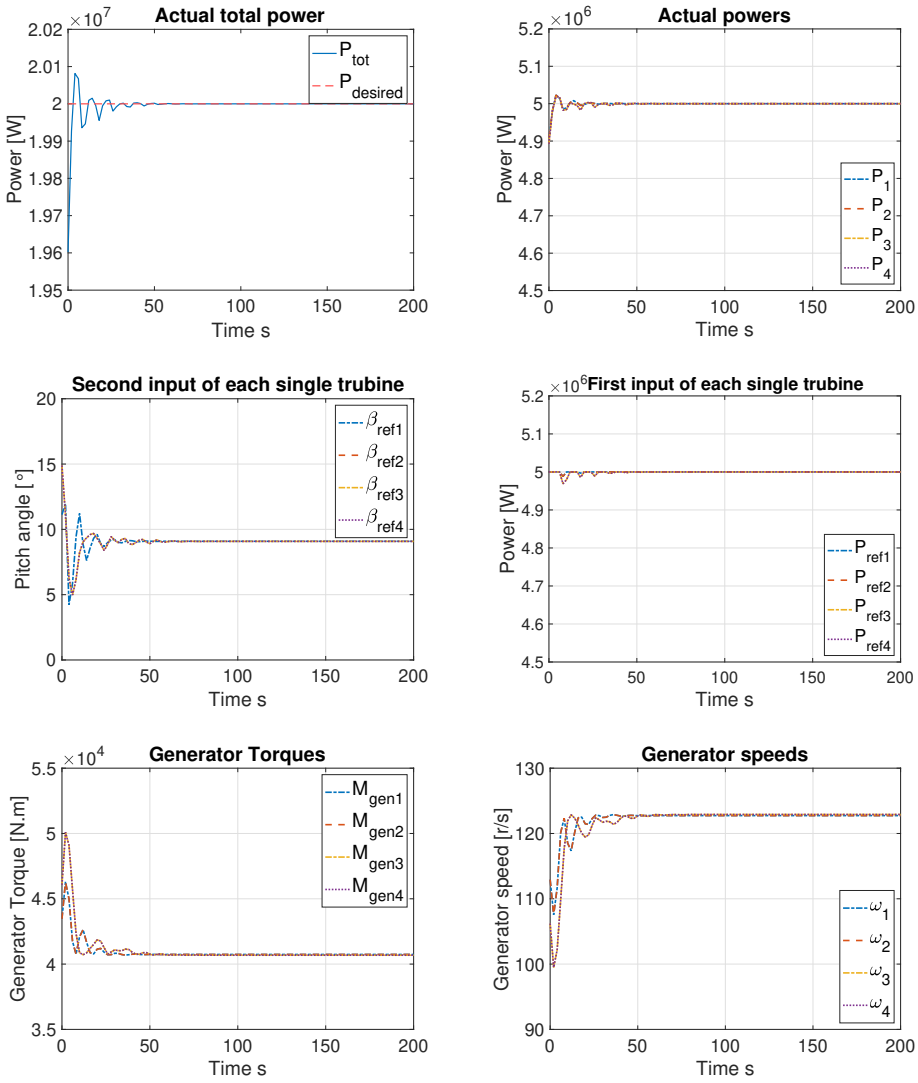

Figure 4.9: The response of NMPC of the FON of 4RT model and reduced-order tower (ROT) model with MDCG (constant wind speed).

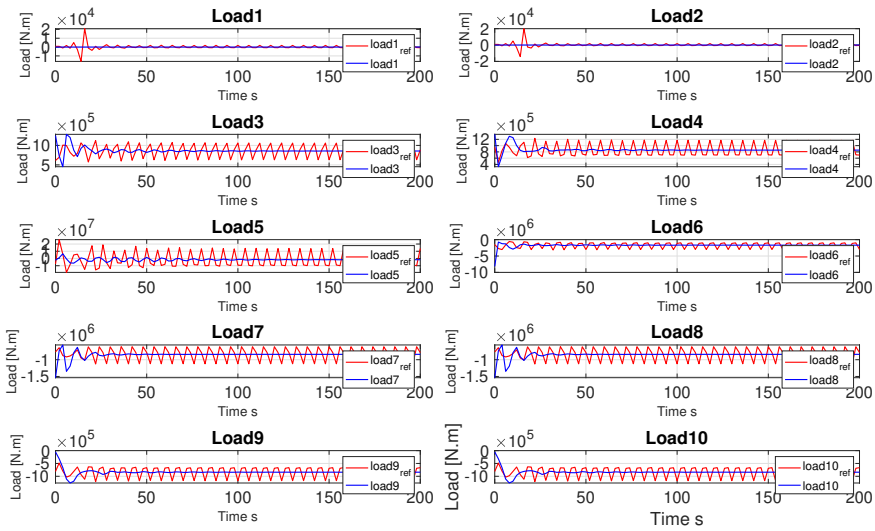

Figure 4.10: Loads on the tower compared to the reference load when NMPC implemented of the FON of 4RT model and reduced-order tower (ROT) model with MDCG (constant wind speed).

4.3 Linear MPC for linearized four-rotor turbine

This section presents the implementation of linear MPC for the linearized model of the 4RT. The constant wind speed (14 $m.s^{-1}$) implemented for the linear MPC. In all scenarios, the actual total power, the actual power of each single turbine, generator torque, and generator speed are plotted from the second time step, where the response for the first step corresponding to the initial states. The reason for this is that we wanted to show how the response changes from the second step. Moreover, in all scenarios, the time step is one second since we chose a prediction horizon of ten seconds and the number of intervals of ten. The result for both full-order and reduced-order of 4RT and tower models are shown in the following sections. Later, the RMSE of total power and load values will be discussed.

4.3.1 Full-order linearized of 4RT and full-order tower models

Fig. 4.11 gives the results of linear MPC, where full-order linearized (FOL) of 4RT and full-order tower (FOT) models are chosen. A good performance of MPC is achieved. The power tracking is good, and the model responds to the jumps in the first input β_{ref} and the second input P_{ref} for each single turbine. Moreover, the generator speed and generator torque fulfill the constraints. The maximum value of generator speed and generator torque are 122.9 r/s and 4.745e+05 $N.m$, respectively.

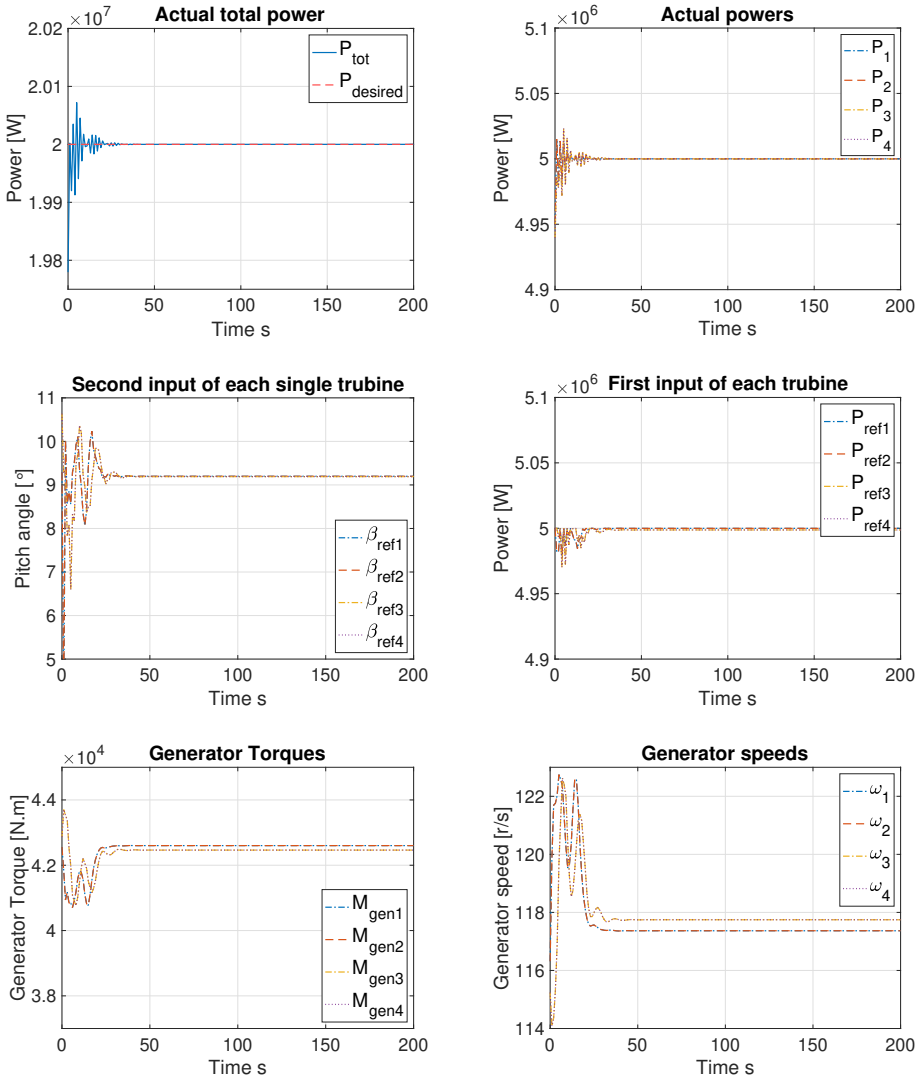

Figure 4.11: The response of linear MPC using the full-order linearized (FOL) of the 4RT and full-order tower (FOT) models.

The load on the tower structure is shown in fig. 4.12. The loads minimized, and the jumps in loads removed compared to the reference loads. The reference loads obtained by running the optimization by removing the load term from the objective function. The linear MPC was faster than NMPC. However, the model suffered from running in real-time. Therefore, there was a need to reduce the model to the fewer states, as we can see in

the next sections.

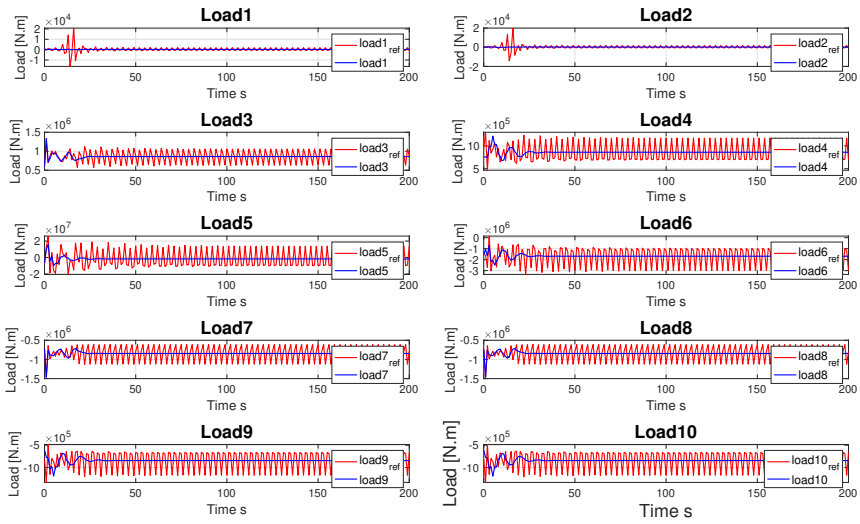

Figure 4.12: Loads on the tower compared to the reference load when linear MPC implemented of using the full-order linearized (FOL) of the 4RT and full-order tower (FOT) models.

4.3.2 Full-order linearized of 4RT and reduced-order tower models

To make the model work in the real-time, the tower model had to be reduced as in section 4.1.1. The tower model is reduced with BT, but it could not be reduced less than 17 states. The response of linear MPC is shown in fig. 4.13. The response is compatible to the full-order tower (FOT) model in section 4.3.1. That validates our results when we did the simulation of full-order and reduced-order tower model with BT. The model responds to the inputs' change in a proper way.

Fig. 4.14 presents the load on the tower. The loads are similar to the loads in the case of the full-order tower model. Moreover, the model is running in the real-time optimization. Thus, the optimal solution found in less than one second.

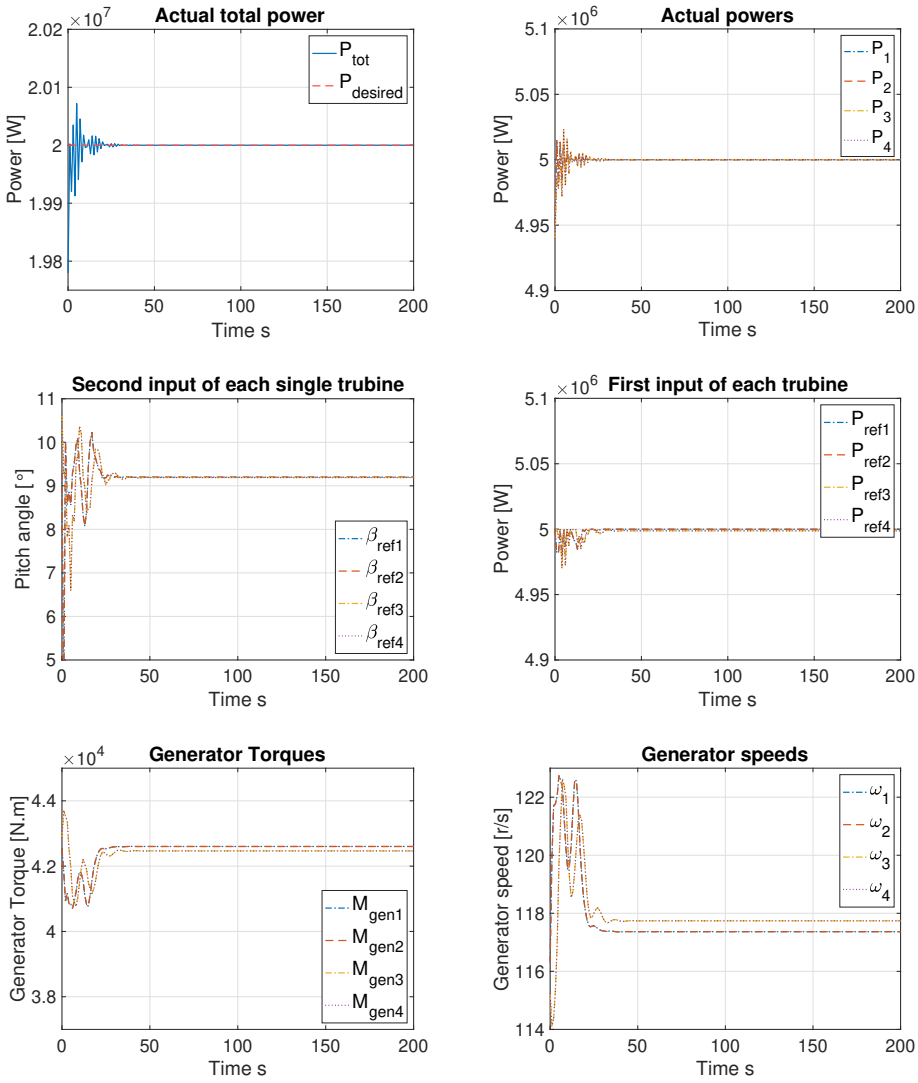

Figure 4.13: The response of linear MPC using FOL of 4RT and reduced-order tower (ROT) with BT.

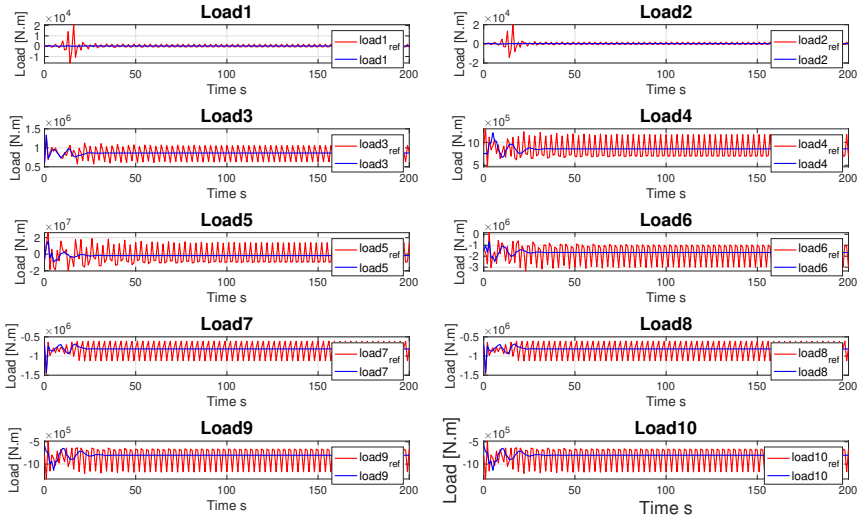

Figure 4.14: Loads on the tower compared to the reference load when linear MPC implemented of the FOL of 4RT and reduced-order tower (ROT) with BT.

Then, the tower model is reduced from 20 to 11 states with MDCG. Fig. 4.15 provides the results of linear MPC with a reduced-order tower (ROT) model. The results are precisely the same as the full-order tower (FOT) model. The optimization was faster than the BT method. The optimal solution also found in less than one second, implying the real-time optimization is achieved. Fig. 4.16 gives the load values, which also are the same as in the full-order model.

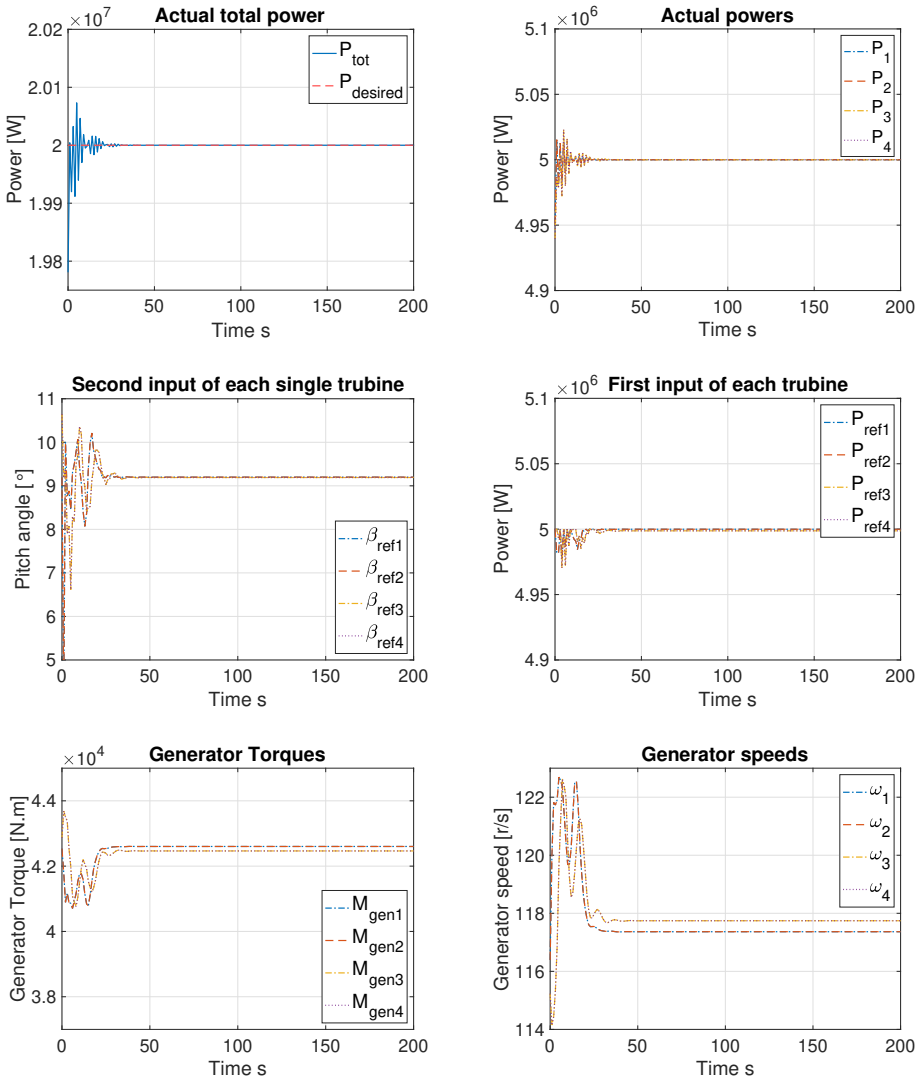

Figure 4.15: The response of linear MPC using the FOL of the 4RT and ROT models using MDCG.

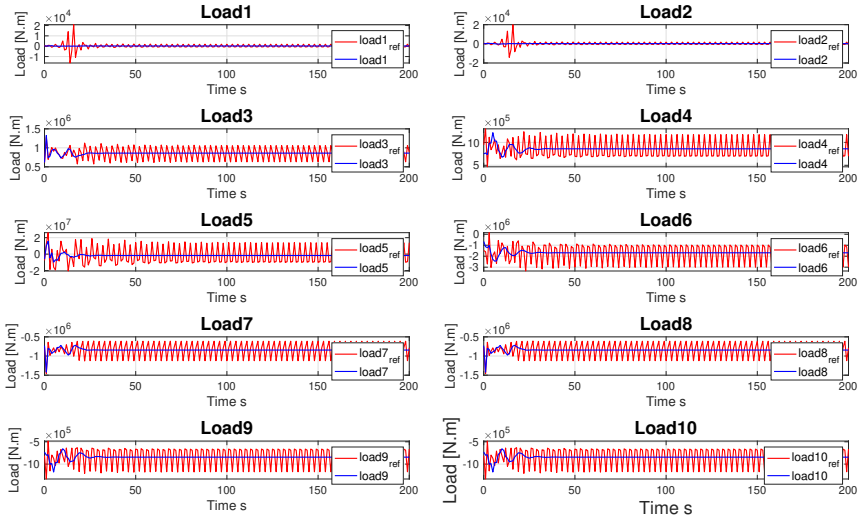

Figure 4.16: Loads on the tower compared to the reference load when linear MPC implemented of using the FOL of the 4RT and ROT models using MDCG.

4.3.3 Reduced-order linearized of 4RT and reduced-order tower models

The linearized model of 4RT reduced from 20 to 4 states with the MDCG method. Then it is implemented with the reduced-order tower (ROT) models. The linear MPC became much faster. Fig. 4.17 shows the response of the reduced-order linearized (ROL) of the 4RT model with MDCG and the reduced-order tower (ROT) model with BT (reduced to 11 states). The model track the changes in the inputs, and the power tracking is perfect, with no jumps over the desired power (20 MW). The loads shows in fig. 4.18, which are minimized with no jumping.

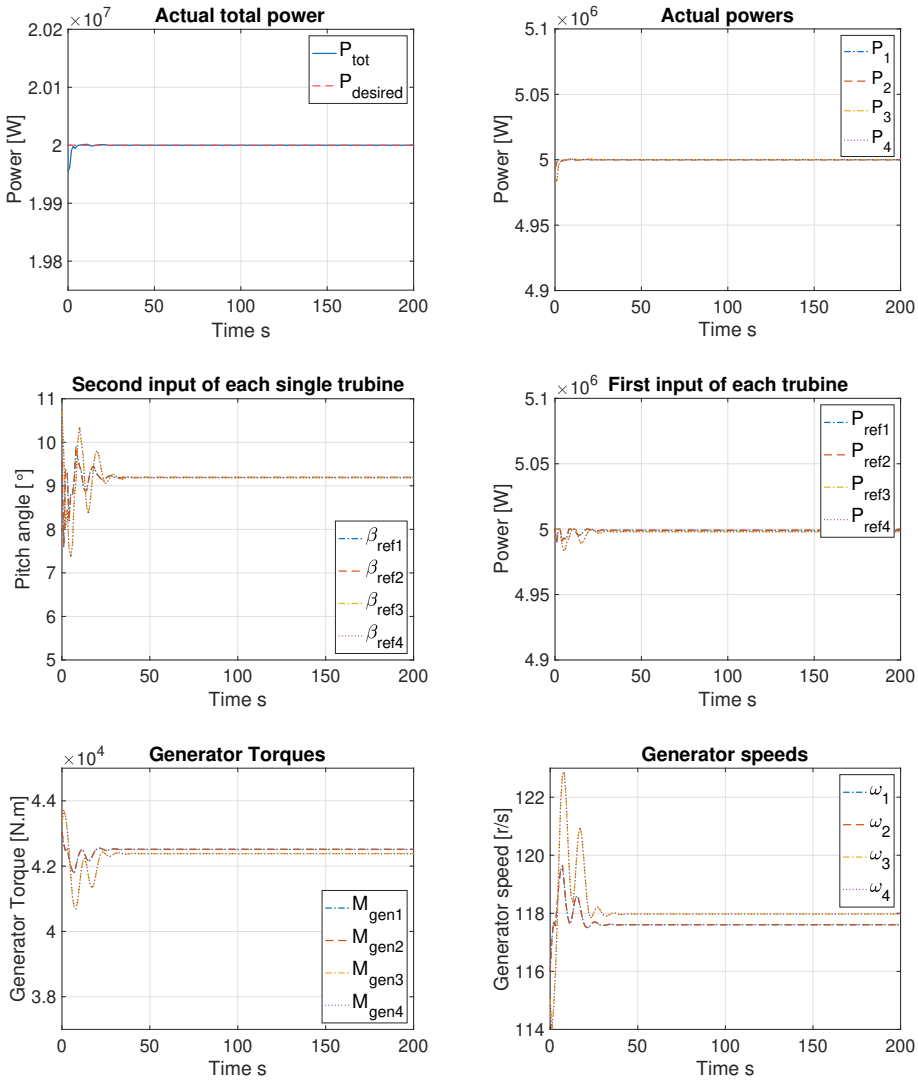

Figure 4.17: The response of linear MPC using reduced-order of linearized 4RT (using MDCG) and reduced-order model of the tower (using BT).

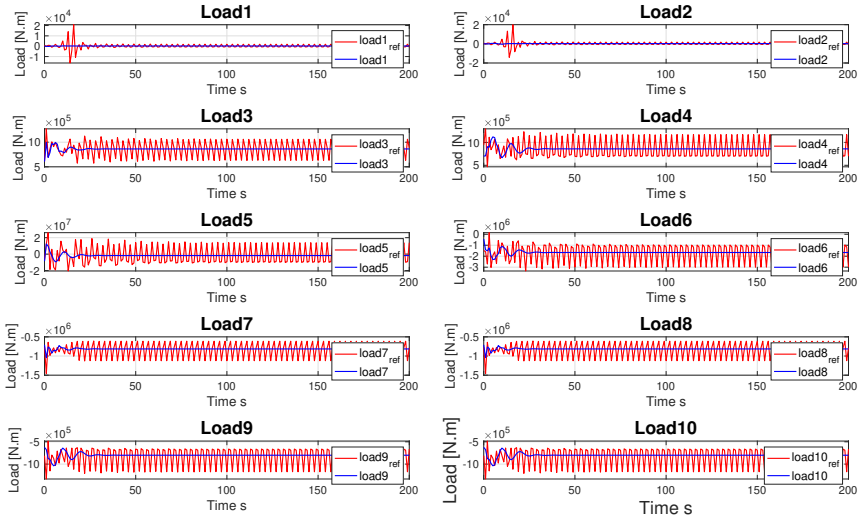

Figure 4.18: Loads on the tower compared to the reference load, when linear MPC implemented of ROL of 4RT model with MDCG and ROT model with BT.

Figs. 4.19 and 4.20 give the response of linear MPC using the ROL of 4RT model with MDCG and reduced-order tower (ROT) model using MDCG. The perfect power tracking is obtained and the loads on tower reduced.

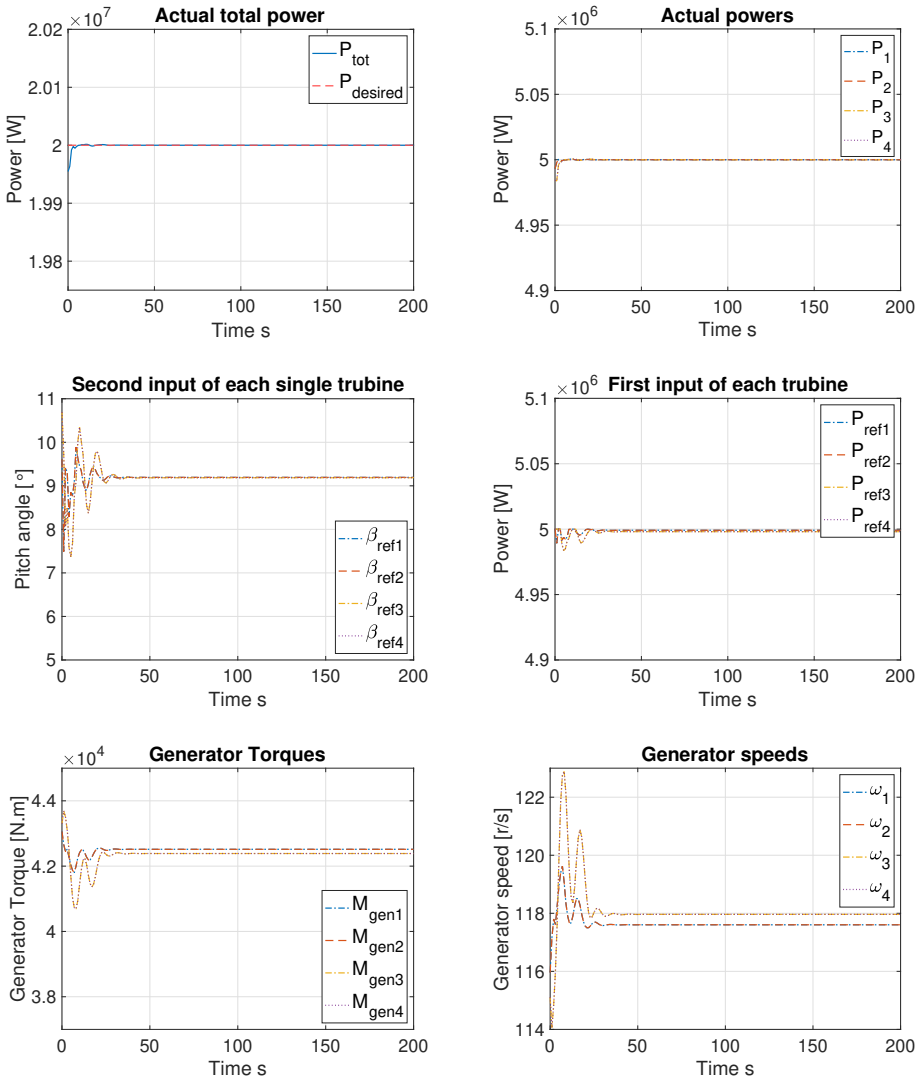

Figure 4.19: The response of linear MPC using ROL of 4RT model with MDCG and ROT model using MDCG.

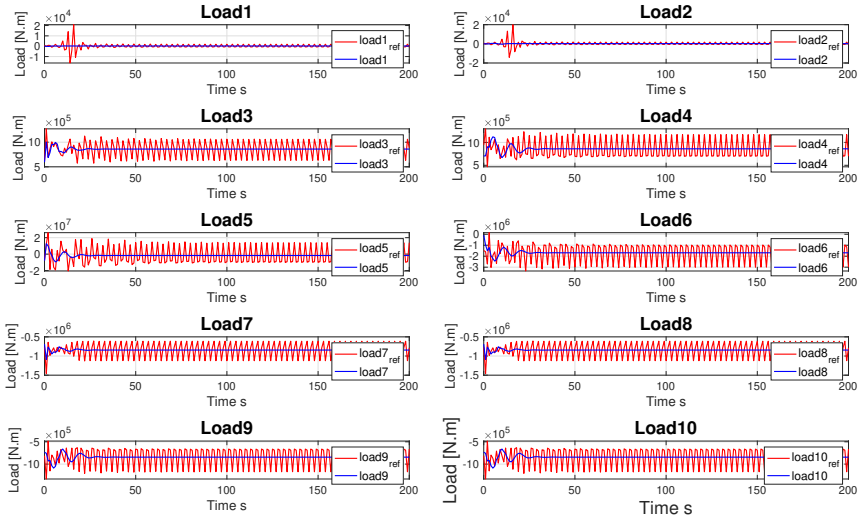

Figure 4.20: Loads on the tower compared to the reference load when linear MPC implemented of the ROL of 4RT model with MDCG and reduced-order tower (ROT) model with MDCG.

4.4 Comparing the results

In this section, we will compare all scenarios by giving the weakness and strengths of each scenario. The comparing will be based on the RMSE of power, RMSE of load, and the computational time.

4.4.1 Power tracking and computational time

Table 4.3 shows the RMSE for power and computational time of all scenarios. The time in table 4.3 refers to the time that MPC took to find the optimal solution. Note that the computational time is computed using a computer with Intel Core i7 3.2 GHz processor. All scenarios can be summarized as follows:

- The NMPC with turbulent wind speeds gave a poor power tracking where RMSE= 58.2e+04 W in the case of FON of 4RT & FOT model and RMSE= 8.61e+04 W in the case of FON of 4RT & ROT model. Wind speeds below the rated wind speed and large MPC's time step caused this degradation in performance. However, the large time step was necessary to reduce computational time. FON of 4RT & ROT model gave better power tracking, lower computational time (reduced to half) than FON of 4RT of 4RT & FOT model. This is due to the shorter time step and wind speeds interpolation. However, no real-time optimization is achieved for both scenarios.

- The NMPC with constant wind speed gave a good power tracking where RMSE= 4.39e+04 W in the case of FON of 4RT & FOT model and RMSE= 4.25e+04 W in the case of FON of 4RT & ROT model. The power tracking is similar between the two scenarios (we used the same time step (2 s)). Nevertheless, the computational time was reduced to half. This is due to reducing the tower model from 20 to 11 states. However, neither scenario could not run in real-time.

- Linear MPC (last 5 rows in table 4.3) provided better power tracking (lower RMSE) than NMPC. This is an unusual result. In general, the nonlinear models give better performance than linear models. The linear models are an approximation of the nonlinear models around the operating points. Nevertheless, our explanations for this unusual result is firstly the length of the time step, and secondly, we decided to use the MPC outputs and not create a feedback plant since feedback resulted in numerical issues. For linear MPC, we chose one second as a time step. Whereas, for NMPC, we chose two or three seconds. Furthermore, the computational time is reduced for linear MPCs. In general, linear MPC is faster than nonlinear MPC. FOL of 4RT and FOT model could not run in real-time (1.5 s). The computational time for a linear model should be less than 1 s to achieve the real-time optimization. All the other four scenarios for linear MPC achieved real-time optimization. The computational time is reduced from scenarios to another, where the states are reduced to fewer numbers. The interesting result is that time is reduced from 0.56 s in the case of FOL of 4RT and ROT (using MDCG) to 0.44 s and 0.27 s in the cases of ROL of 4RT (using MDCG) and ROT(using BT) and ROL of 4RT (using MDCG) and ROT(using MDCG), respectively. When the states are reduced from 20 to 4 for 4RT, but the time did not reduce by much. The explanation for that is we added more constraints to ROL of the 4RT model (using BT and MDCG) to fulfill the constraints on the states and extra constraints lead to larger computational time.

- Linear MPC scenarios (ROL of 4RT & ROT (with BT and MDCG method)) gave a better power tracking and shorter computational time than linear MPC scenarios (FOL of 4RT & FOT and FOL of 4RT & ROT).

RMSE of power in Watts and computational time in seconds		
Model	RMSE	time
FON of 4RT & FOT (turbulent wind)	58.2e+04 W	31.9 s
FON of 4RT & FOT (constant wind)	4.39e+04 W	7.1 s
FON of 4RT & ROT (using MDCG) (turbulent wind)	8.61e+04 W	14.3 s
FON of 4RT & ROT (using MDCG) (constant wind)	4.25e+04 W	3.6 s
FOL of 4RT & FOT (full-order)	1.96e+04 W	1.5 s
FOL of 4RT & ROT (using BT)	1.95e+04 W	0.71 s
FOL of 4RT & ROT (using MDCG)	1.95e+04 W	0.56 s
ROL of 4RT (using MDCG) & ROT (using BT)	0.42e+04 W	0.44 s
ROL of 4RT (using MDCG) & ROT (using MDCG)	0.41e+04 W	0.27 s

Table 4.3: RMSE between the actual and desired power 20 MW.

4.4.2 load on tower structure

Reducing the load on the tower's structure is important to keep the whole plant operating under safe conditions. We tried to choose the weights on the load and power terms to keep power tracking and reduce the load on the structure. We have ten loads on the tower which was derived and explained in sections 2.4.3 and 2.4.4. Tables 4.5 and 4.4 present the RMSE between actual and reference load in case of linear MPC and NMPC, respectively. As we mentioned before, we chose two reference loads. One of them is for the case of turbulent wind speed, and another is for constant wind speed (both linear MPC and NMPC). We found the reference load by removing the load term from the objective function and running the optimization for turbulent and constant wind speeds. Nevertheless, the loads had to be compared to the result of another controller or reference values. Due to the time restriction, we created a reference from our MPC. Note that the higher the RMSE value, the better load reduction. This is based on our assumption of the reference load, which was higher than the loads in our different scenarios. The results of load reduction can be

summarized as:

- Table 4.4 shows that in the case of NMPC with the turbulent wind speeds, the RMSE is low. This implies that load reduction is poor. We had to sacrifice the load reduction to get better power tracking. Therefore, more significant weight on the power term is used compared to the constant wind speed scenarios, explaining the poorness in load-reducing. Another explanation is that different wind speeds (high wind speeds) give poorness in load reduction.
- Table 4.4 presents the RMSEs of NMPC in case of constant wind speed. The RMSEs are higher (better load-reducing) than the turbulent case. The reason for that is in the choice of the weights and constant wind speed is used.
- The RMSEs are high and compatible in all linear MPC's scenarios, as shown in table 4.5. This implies there was a balance of choosing weights and reduced-order methods did not cause to reduce the MPC's performance.
- The load reduction in the NMPC in case of constant wind speed is better than some linear MPC scenarios (FOl of 4RT & FOT, FOl of 4RT & ROT (with BT and MDCG methods)). The load reduction is close to other linear MPC scenarios (ROl of 4RT & ROT (with BT and MDCG methods))

RMSE of loads of NMPC				
Loads	FON 4RT & FOT (turbulent wind)	FON 4RT & ROT (turbulent wind)	FON 4RT & FOT (constant wind)	FON 4RT & ROT (constant wind)
Load1	1.19	0.77	1.39	1.42
Load2	1.11	1.02	1.47	1.38
Load3	1.11	1.01	1.46	1.45
Load4	0.86	0.91	1.33	1.31
Load5	1.36	1.09	1.41	1.41
Load6	1.05	0.58	1.46	1.44
Load7	1.18	0.59	1.39	1.38
Load8	0.99	1.19	1.39	1.38
Load9	1.08	1.07	1.34	1.32
Load10	0.71	1.12	1.34	1.32

Table 4.4: RMSE between the actual load on tower and the reference load in case of NMPC.

RMSE of loads of linear MPC					
Loads	FOL 4RT & FOT	FOL 4RT & ROT (BT)	FOL 4RT & ROT (MDCG)	ROL 4RT (MDCG) & ROT (BT)	ROL 4RT (MDCG) & ROT (MDCG)
Load1	1.19	1.19	1.29	1.42	1.44
Load2	1.38	1.38	1.42	1.43	1.43
Load3	1.23	1.23	1.23	1.26	1.26
Load4	1.37	1.37	1.36	1.39	1.39
Load5	1.22	1.22	1.22	1.27	1.26
Load6	1.31	1.31	1.36	1.34	1.35
Load7	1.26	1.26	1.26	1.28	1.28
Load8	1.26	1.26	1.26	1.28	1.28
Load9	1.38	1.38	1.38	1.41	1.41
Load10	1.38	1.38	1.38	1.41	1.41

Table 4.5: RMSE between the actual load on tower and the reference load in case of linear MPC.

Chapter 5

Discussion

The work in this thesis achieved substantial goals in model reduction, producing real-time models, in exploring techniques used in these systems and has some limitations. These are summarised below:

5.1 Turbulent and constant wind speeds

Turbulent and constant wind speeds are applied to the NMPC. Whereas only the constant wind speed was applied to the linear MPC. The linear models (both full-order and reduced-order) had to be interpolated for different wind speed to be able to handle turbulent wind speeds. However, due to time restriction, the interpolation of linear models was not performed.

5.2 Reduced-order model and real-time optimization

Reduced-order model enables the MPC to work in real-time. However, this reduction of the order did not affect the performance of the model. The MDCG method was more efficient than BT. Efficiency means that the model could be reduced to fewer states, reducing the computational time. Nevertheless, the performance of the models did not decrease.
The real-time running could not be fulfilled in all scenarios of NMPC. However, all scenarios of linear MPC with reduced-order model allowed the real-time running.

5.3 Power tracking

To measure the power tracking, we used RMSE to calculate the error between the actual and desired power. This was shown in table 4.3 for all scenarios.

- The NMPC with turbulent wind speeds gave a poor power tracking. The real-time optimization could not be achieved.
- The NMPC with the reduced-order tower (ROT) model provided a better power tracking than NMPC with the full-order tower (FOT) model. The smaller time step used in case of reduced-order and the wind speed interpolation are the explanation for different behavior. Nevertheless, the real-time optimization could not be fulfilled.
- The best power tracking was fulfilled with the linear MPC. This tracking was better than the NMPC. Choosing the proper time step and using the MPC outputs and not create a feedback plan made the linear MPC better. In addition, real-time optimization was fulfilled in all linear MPC scenarios after reduction the order of the tower or/and 4RT. That was not the case for NMPC.

5.4 Load on tower structure

The results of load reduction can be summarized as:

- NMPC in the case of the turbulent wind speeds gave a poor load reduction. We are sacrificing the load reduction to get better power tracking.
- The load reduction of NMPC in case of constant wind speed was better than the turbulent wind speeds case. Two reasons for that. Firstly, there are the different input wind speeds since we used constant wind speed vs turbulent wind speeds. Secondly, the choice of the weights on load and power terms.
- The RMSEs are high and almost are the same in all linear MPC's scenarios,i.e, better load reduction is achieved. That implies there was a balance of choosing weights and reduced-order methods that did not cause to reduce the MPC's performance.
- The load reduction in NMPC in case of constant wind speed are close to the load reduction in linear MPC.

Chapter 6

Conclusion and further work

6.1 Conclusion

In this thesis, the nonlinear MPC (NMPC) was developed for the four-rotor turbine (4RT). The main goal of MPC was to track the power reference and to reduce the load on the tower structure. The MPC should work in real-time. So the limitations were found; for example, the NMPC could not track the power in case of turbulent wind speeds. Moreover, the load reduction was not promising. No real-time optimization was achieved. Then, the NMPC with constant wind speed is tested. Poor power tracking was found for the case of the full-order tower, but better power tracking was obtained in case reduced-order tower. The NMPC, in the case of constant wind speed, gave better power tracking and good load reduction. Nevertheless, the NMPC could not achieve real-time performance. Then the nonlinear model of the four-rotor turbine was linearized.
The linear MPC was developed. The full-order linear four-rotor turbine and full-order tower models were tested. Good power tracking and load reduction were obtained without real-time optimization. Then, the tower model was reduced from 20 to 17 states with balanced truncation and from 20 to 11 states using the matched DC gain method. Moreover, the linearized 4RT was reduced from 20 to 4 states using matched DC gain. The simulation and optimization were done to ensure that the full-order and reduced-order models have similar performance; the results of simulation and optimization showed that the full-order and reduced models are similar. Then different scenarios of linear MPC was performed. All scenarios gave a good power tracking, good load reduction and real-time optimization was achieved. However, the scenarios with reduced-order of 4RT gave better power tracking and reduction than all other scenarios of linear MPC, where the full-order linearized 4RT was implemented.

To conclude, the matched DC gain method of order reduction was more efficient than the balanced truncation method since the model could be reduced to fewer states, i.e., reducing the computational time. The reduced-order model represented the full-order model with sufficient accuracy. The linear MPC was better than NMPC in both performance and computational time.

6.2 Future work

Many options can be done in the further from this thesis.

- Comparing the loads on the tower with another controller, such as the Vestas controller [15].
- Interpolating the linearized 4RT model at different wind speeds. In this case, the turbulent wind speeds can be utilized for linear MPC. The interpolation did not achieved due to time restriction.
- In this thesis, wind speeds and all states assumed to be measurable. Modern wind turbines operate in a wide range of wind speeds. To enable wind turbine operation in such a variety of operating conditions, sophisticated control and estimation algorithms are needed. Thus, an extended Kalman filter can be used to estimate the unmeasurable states and wind speed using only available sensors.

References

[1] Aeolus, 2012. Creating a wind field. http://www.ict-aeolus.eu/SimWindFarm/windfield.html. Accessed: 2020-03-02.

[2] Andersson, J., 2013. A General-Purpose Software Framework for Dynamic Optimization. PhD thesis. Arenberg Doctoral School, KU Leuven. Department of Electrical Engineering (ESAT/SCD) and Optimization in Engineering Center, Kasteelpark Arenberg 10, 3001-Heverlee, Belgium.

[3] Bianchi, F.D., De Battista, H., Mantz, R.J., 2006. Wind turbine control systems: principles, modelling and gain scheduling design. Springer Science & Business Media.

[4] Datta, B., 2004. Numerical methods for linear control systems. volume 1. Academic Press.

[5] Diehl, M., ESAT-SCD, K., 2011. Numerical optimal control draft.

[6] Fortes Plaza, A., 2017. Development of reduced order models for wind farm control. Master's thesis. Universitat Politècnica de Catalunya.

[7] Foss, B., Heirung, T.A.N., 2013. Merging optimization and control. Lecture Notes .

[8] Gressick, W., Wen, J.T., Fish, J., 2005. Order reduction for large-scale finite element models: A systems perspective. International Journal for Multiscale Computational Engineering 3.

[9] Grunnet, J.D., Soltani, M., Knudsen, T., Kragelund, M., Bak, T., 2010. Aeolus toolbox for dynamic wind farm model, simulation and control, in: Proc. of the 2010 European Wind Energy Conference.

[10] Henriksen, L.C., 2011. Model predictive control of wind turbines .

[11] IEA, 2019. international energy agency world energy outlook 2019. https://www.iea.org/weo2019/. Accessed: 2020-06-01.

[12] Jamieson, P., Branney, M., 2012. Multi-rotors; a solution to 20 mw and beyond? Energy Procedia 24, 52–59.

[13] Jonkman, J., Butterfield, S., Musial, W., Scott, G., 2009. Definition of a 5-MW reference wind turbine for offshore system development. Technical Report. National Renewable Energy Lab.(NREL), Golden, CO (United States).

[14] Kale, S.A., Sapali, S., 2013. A review of multi-rotor wind turbine systems. Journal of sustainable manufacturing and renewable energy 2, 3.

[15] Knudsen, T., Filsoof, O.T., Hovgaard, T.G., Grunnet, J.D., Neto, J.X.V., Wisniewski, R., et al., 2018. Multi-rotor wind turbine control challenge-a benchmark for advanced control development, in: 2018 IEEE Conference on Control Technology and Applications (CCTA), IEEE. pp. 1615–1622.

[16] Manrique, R., Sofrony, J., . Data-driven fault detection and isolation: A wind turbine scenario .

[17] MathWorks, 2020. Root mean square calculation. https://www.mathworks.com/help/signal/ref/rms.html. Accessed: 2020-05-05.

[18] Mehrmann, V., Stykel, T., 2005. Balanced truncation model reduction for large-scale systems in descriptor form, in: Dimension Reduction of Large-Scale Systems. Springer, pp. 83–115.

[19] Neogi, S., 2017. Automatic tuning of wind tubrine controller .

[20] Seborg, D.E., Mellichamp, D.A., Edgar, T.F., Doyle III, F.J., 2010. Process dynamics and control. John Wiley & Sons.

[21] Silveira, L.M., 1994. Model order reduction techniques for circuit simulation. Ph.D. thesis. Massachusetts Institute of Technology.

[22] Tailor, M.R., Bhathawala, P., 2011. Linearization of nonlinear differential equation by taylor's series expansion and use of jacobian linearization process. International Journal of Theoretical and Applied Science 4, 36–38.

[23] ukić, S.D., Sarić, A.T., 2012. Dynamic model reduction: An overview of available techniques with application to power systems. Serbian journal of electrical engineering 9, 131–169.

[24] Verma, P., 2013. Multi rotor wind turbine design and cost scaling .

[25] Wikipedia, 2018. Global wind power cumulative capacity. https://no.wikipedia.org/wiki/Fil:Global_Wind_Power_Cumulative_Capacity.svg. Accessed: 2020-06-02.

[26] Yuan, Y., Tang, J., 2017. On advanced control methods toward power capture and load mitigation in wind turbines. Engineering 3, 494–503.

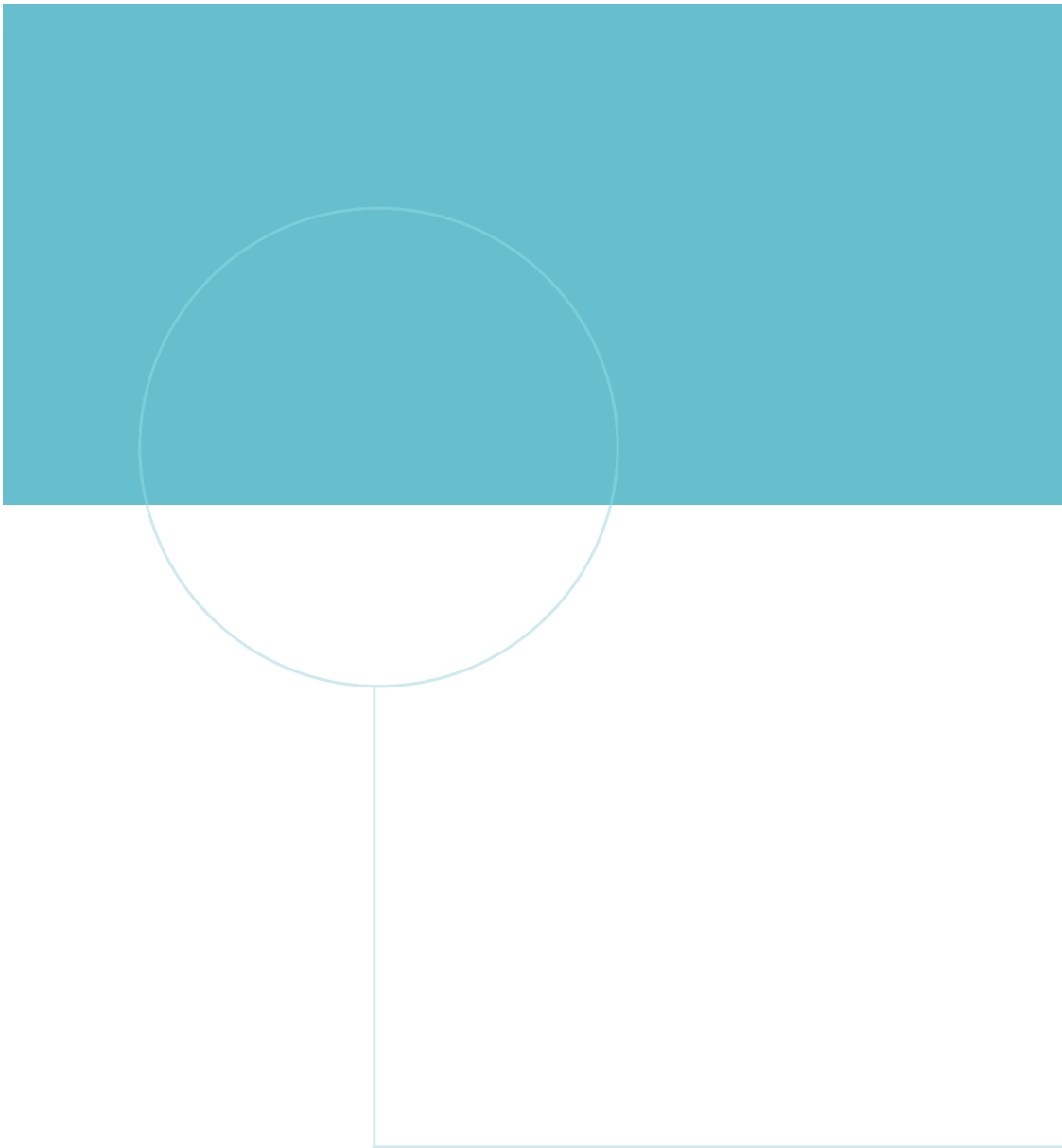

NTNU

Norwegian University of
Science and Technology